MODELLING THE WAVE DYNAMICS OF SOLAR ATMOSPHERE TO STUDY CORONAL HEATING

MSc Astronomy Thesis

By

Devesh Sharma



DEPARTMENT OF ASTRONOMY , ASTROPHYSICS AND SPACE ENGINEERING

INDIAN INSTITUTE OF TECHNOLOGY INDORE

May, 2025

MODELLING THE WAVE DYNAMICS OF SOLAR ATMOSPHERE TO STUDY CORONAL HEATING

A THESIS

Submitted in partial fulfilment of the requirements for the award of the degree

of

Master of Science

by

Devesh Sharma



DEPARTMENT OF ASTRONOMY , ASTROPHYSICS AND SPACE ENGINEERING

INDIAN INSTITUTE OF TECHNOLOGY INDORE

May, 2025



INDIAN INSTITUTE OF TECHNOLOGY INDORE

CANDIDATE'S DECLARATION

I hereby certify that the work which is being presented in the thesis 'Modelling the wave dynamics of solar atmosphere to study coronal heating'. in the partial fulfillment of the requirements for the award of the degree of MASTER OF SCIENCE and submitted in the DEPARTMENT OF ASTRONOMY, ASTROPHYSICS AND SPACE ENGINEERING, Indian Institute of Technology Indore, is an authentic record of my own work carried out during the time period July 2025 to May 2025 under the supervision of Dr. Bhargav Vaidya

The matter presented in this thesis has not been submitted by me for the award of any other degree of this or any other institute.

Signature of the student with date **DEVESH SHARMA**

This is to certify that the above statement made by the candidate is correct to the best of my/our knowledge.

10/05/2025

Signature of the Supervisor of M.Sc. thesis (with date) **Dr. Bhargav Vaidya**

Devesh Sharma has successfully given his/her M.Sc. Oral Examination held on 05/05/2025

10/05/2025

Mansuela Chakrakosty

Signature(s) of Supervisor(s) of MSc thesis

Date:

Programme Coordinator, M.Sc.

Manoueta Chakrakorty

Date: 19/05/2025

Convenor, DPGC

Date: 19/05/2025

HoD, DAASE

Date:

ACKNOWLEDGEMENT

I would like to express my deepest gratitude to my supervisor, Dr. Bhargav Vaidya, for granting me the opportunity to work on this project. His invaluable guidance in numerical modeling, constant support, and the freedom he provided throughout this work have been instrumental in shaping both this project and my academic journey. I am especially grateful for his motivation to participate in conferences and workshops, which played a significant role in refining my scientific interests and research goals.

I am immensely thankful to my colleagues from the lab, whose constant help, insightful discussions, and camaraderie made this experience fulfilling and enjoyable. Without their support, it would have been difficult to carry out this work as smoothly. I am equally grateful to all my batchmates and friends for their encouragement, companionship, and for making this journey memorable.

A special note of thanks to Dr. Raj Joshi, whose expertise and assistance with the PLUTO code helped me navigate many challenges, from which I learned a great deal. I am also sincerely thankful to Dr. Samuel Skirvin, with whom I had engaging discussions on MHD waves that deepened my understanding of it. His guidance played an important role in helping me set up and comprehend key aspects of this work.

I owe my heartfelt gratitude to my parents, whose unwavering love, encouragement, and belief in me have been my greatest strength. Their support in both moments of failure and success has been invaluable throughout my life.

I am grateful to the **Department of Astronomy, Astrophysics and Space Engineering** for providing me with the platform to contribute to this fascinating and dynamic field.

Lastly, I want to acknowledge my past self for having the courage to embark on this journey into Astronomy. It was a difficult decision, but one that gave my present and future self the belief and confidence to pursue my dreams without doubting my own capabilities.

ABSTRACT

Heating in the solar atmosphere has long remained one of the central unsolved problems in solar physics. Despite significant progress in both observational capabilities and theoretical modeling, the precise mechanisms responsible for maintaining the high coronal temperatures continue to be debated. Among the proposed candidates, wave heating — particularly via pmode-driven magnetohydrodynamic (MHD) waves interacting with structured magnetic fields — has attracted increasing interest. In this thesis, we present a comprehensive study of MHD waves through 2.5D MHD simulations to examine the influence of various wave drivers and magnetic field configurations on wave propagation, mode coupling, and energy transport in the solar atmosphere. Our results show that employing a realistic broadband driver for p-mode oscillations produces power spectra peaking around 4 mHz which is in close agreement with observations. Furthermore, we also simulated the solar jets and studied the wave generation and how it is influced under the p-mode oscillations. It was found that p-mode like oscillations can also enhance the high frequency transverse oscillations in chromosphere and generate coronal power spectrum with frequncy peaking at around 3.5-3.7 mHz. These results provide further insight on the role of wave-driven processes in coronal heating and highlight the dynamic coupling between photospheric motions and coronal oscillations.

Contents

Li	st of l	Figures	IX
1	Intr	oduction	1
	1.1	Understanding the Sun's Atmosphere	1
	1.2	Structure of the solar atmosphere	2
	1.3	Coronal heating	7
		1.3.1 Heating Mechanisms	8
	1.4	Solar Oscillations	9
		1.4.1 <i>p</i> -mode oscillations	12
	1.5	Magneto-hydrodynamic Waves	13
		1.5.1 Mode Conversion in the Solar Atmosphere	17
		1.5.2 Interaction with jets	19
	1.6	Previous works	19
	1.7	Objectives	22
2	Met	hodology	23
	2.1	PLUTO code	24
	2.2	Numerical Setup	25
		2.2.1 Initial Condition	25
		2.2.2 Boundary Conditions	28
		2.2.3 Photospheric Driver	29
	2.3	Launching Solar Jet	30
	2.4	Analysis	32
3	Resi	ults and Discussions	34
	3.1	Monochromatic driver	34
		3.1.1 Vertical magnetic field	35
		3.1.2 Arcade magnetic field	38
	3.2	Broadband driver	41
		3.2.1 Vertical magnetic field	41

		3.2.2	Arcade magnetic field	44
	3.3	Transi	ent events (Solar jets)	47
		3.3.1	Solar Jet Launch and Wave Evolution	47
		3.3.2	Solar Jets under the Influence of <i>p</i> -Mode Oscillations	49
4	Sum	mary &	& Outlook	51
	4.1	Summ	ary	51
	4.2	Future	Work	52
Bi	hliogi	ranhv		54

List of Figures

1.1	Total solar eclipse during Aug. 21, 2017, showing the phases of the eclipse and	
	the prominences erupting out of the sun are seen clearly during a total eclipse.	
	It is red because of Lyman α emission. (Image Credit: Jay Pasachoff, Ron	
	Dantowitz, Christian Lockwood)	1
1.2	This plot illustrates the variation of temperature and density with height in the	
	solar atmosphere. The orange peaks correspond to spicules extending from the	
	chromosphere into the lower corona. The dark yellow band marks the transition	
	region — a narrow layer, only a few hundred kilometers thick, that closely	
	follows the spicule structures. This region serves as a boundary separating the	
	cooler, denser chromosphere from the hotter, more rarefied corona. This image	
	is taken from book New Sun: The Solar Results From Skylab. by Eddy and Ise	
	(1979)	4
1.3	Here we can see the transient forest of spicules and they are spread all over the	
	solar surface. Image is taken by SDO AIA on 2024-5-21 in 304nm He II lines.	
	Image of Earth is for scale	5
1.4	Ground-based observations of active-region flows. Image is taken from book	
	Solar Magnetohydrodynamics by Priest (2014)	5
1.5	Observations taken on 21-5-2-2024 by SDO AIA (Image on the left and bottom	
	right) and Hinode (top right) showing the transient feature of the sun. We can	
	observe (a) a coronal hole, (b) coronal loops, (c) prominence, (d) X-Ray bright	
	points in the XRT image by Hinode, and (e) a filament structure hanging in the	
	corona. Priest (2014)	6

1.6	Wave propagation diagram for the sun. X-axis represents the radial distance distorted to emphasize different layers. Solid line represents the Brunt-Väsälä buoy ancy frequency, dashed line represents the cut-off frequency and dotted line is	/-
	the dispersion relation for waves in spherical geometry as of in stars (Leibacher	
	and Stein (1981)). This diagram represents the types of waves trapped in differ-	
	ent resonant cavities in the Sun. In the interior of the Sun, g-modes are trapped	
	with theoretical time period of 40 minutes. Near the solar surface, p-modes of	
	5-minute time period is trapped and in chromosphere 3-minute oscillations are	
	trapped	11
1.7	Plot for phase velocity (relative to v_A) vs angle for slow, fast and Alfvén mode	11
1./		16
1 0	for a system where $v_A = 0.7c_s$, $v_A = c_s$ and $v_A = 1.2c_s$	10
1.8	How particles oscillate in different modes of MHD waves in 3D, along with	
	their 2D slices to understand the motion of particles better. Vectors represent	17
1.0	the direction magnetic field and wave propagation.	17
1.9	Plasma beta profile over an active region of the sun. The plasma beta is shown	10
1 10	as the shaded region Gary (2001)	18
1.10		
	line width (red) as measured by the COMP instrument. The Doppler velocity	
	spectrum clearly shows a strong and broad peak around 3.5 mHz, indicating	
	dominant oscillations at this frequency. Tomczyk et al. (2007)	20
2.1	Initial profile of hydrostatic solar atmosphere	26
2.2	Plot for density height scale	27
2.3	Initial profile for stratified atmosphere with oblique magnetic field	27
2.4	Initial profile for stratified atmosphere with arcade magnetic field	28
2.5	BiSON spectrum of p-mode oscillation, Elsworth et al. (2015)	30
2.6	Broad-band power spectrum and velocity timeseries	31
3.1	Temporal evolution of temperature and density profiles under the influence of	
	a monochromatic driver in an arcade magnetic field configuration	34
3.2	Temporal evolution of MHD variables at the center of the domain for a vertical	
	magnetic field subjected to a monochromatic driver	35
3.3	Normalized power spectrum of MHD wave variables for a vertical magnetic	
	field with a monochromatic driver, showing a dominant peak at 3.2 mHz	36
3.4	Energy flux components associated with slow, fast, and Alfvén modes in a	
	vertical magnetic field driven by a monochromatic driver	37
3.5	Acoustic, magnetic and total energy flux as a function of height for a vertical	
	magnetic field with a monochromatic driver.	37

3.6	Temporal evolution of MHD wave variables at the center of the domain for an arcade magnetic field driven by a monochromatic source	38
3.7	Normalized power spectrum of MHD wave variables for an arcade magnetic	
	field with a monochromatic driver, highlighting a peak at 3.2 mHz	39
3.8	Energy flux components associated with slow, fast, and Alfvén modes in an	
	arcade magnetic field driven by a monochromatic driver	40
3.9	Acoustic, magnetic and total energy flux as a function of height for an arcade	
	magnetic field with a monochromatic driver	40
3.10		
	a broadband driver.	41
3.11	Temporal evolution of MHD wave variables at the center of the domain for a	
	vertical magnetic field driven by a broadband source	41
3.12	Normalized power spectrum of MHD wave variables for a vertical magnetic	
	field with a broadband driver, showing a shift in peak power towards 4 mHz	42
3.13	Energy flux components for slow, fast, and Alfvén modes in a vertical magnetic	
	field driven by a broadband driver.	43
3.14	Acoustic, magnetic and total energy flux as a function of height for a vertical	
	magnetic field with a broadband driver	43
3.15	Temporal evolution of MHD wave variables at the center of the domain for an	
	arcade magnetic field driven by a broadband source	44
3.16	Normalized power spectrum of MHD wave variables for an arcade magnetic	
	field with a broadband driver	45
3.17	Energy flux components for slow, fast, and Alfvén modes in an arcade magnetic	
	field driven by a broadband driver.	46
3.18	Acoustic, magnetic and total energy flux as a function of height for an arcade	
	magnetic field with a broadband driver	46
3.19	Time evolution of a solar jet driven by a pressure-pulse perturbation in an ar-	
0125	cade magnetic field. The panels show the progression of the jet at successive	
	time frames	47
3.20	Temporal evolution of slow and fast MHD energy flux components following	- /
	the launch of a jet in an arcade magnetic field without p-mode oscillations	48
3.21	Power spectra of MHD wave modes generated by a jet in the absence of p-mode	
0.21	oscillations.	48
3.22	Temporal evolution of slow and fast MHD flux components for a jet launched	
	in the presence of p -mode oscillations in an arcade magnetic field	49
3.23	Power spectra for for slow and fast MHD components generated by jet launch	.,
 -	along with p-mode oscillations	50
	o p ==== == = = = = == == = = = = =	

Chapter 1

Introduction

1.1 Understanding the Sun's Atmosphere

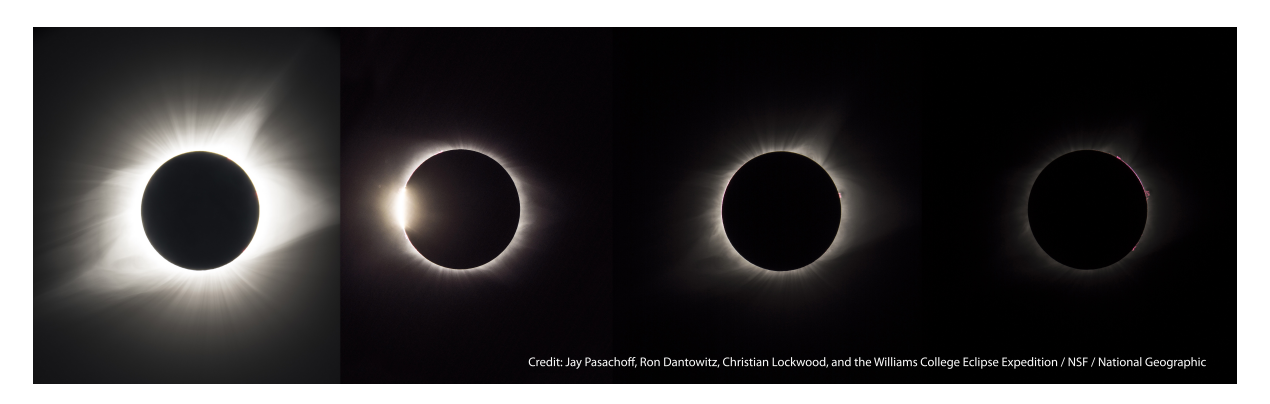


Figure 1.1: Total solar eclipse during Aug. 21, 2017, showing the phases of the eclipse and the prominences erupting out of the sun are seen clearly during a total eclipse. It is red because of Lyman α emission. (Image Credit: Jay Pasachoff, Ron Dantowitz, Christian Lockwood)

The journey of understanding the sun, our neighboring star, is deeply rooted in the history of humanity, where early observations were primarily limited to tracking the sun's visible path across the sky. Solar eclipses provided brief glimpses of the sun beyond its visible disk. As shown in 1.1, the sun also has structures beyond the photosphere, which are usually not visible to our eyes under normal conditions. In the 17th century, Galileo Galilei, using his telescope, observed the sunspots over time and revealed that the sun is a dynamic object that evolves with time. By the 19th century, advancements in spectroscopy opened new avenues into solar composition, leading to the discovery of the sun's hydrogen and helium-rich nature; indeed, helium was first identified in the solar spectrum.

In 1869, American astronomers Charles Young and William Harkness detected an anomalous green spectral line at 530.3 nanometers. Initially, this line was believed to originate from an unidentified element, which was designated as *coronium*. However, in 1942, a significant breakthrough occurred when Bengt Edlén identified that *coronium* was not a new element, but

rather a highly ionized form of iron, Fe¹³⁺ (Edlén (1942)). Such high orders of ionization would require about 500 eV, which cannot be supplied by radiation coming from the photosphere. He determined that the temperature needed to supply that energy must be of the order of a million Kelvins. This conundrum is what we know as the *coronal heating problem*, raising profound questions about the mechanisms that power the sun's atmosphere and initiating a search for answers that continues to drive solar physics research today Edlén (1942); De Moortel et al. (2020).

1.2 Structure of the solar atmosphere

Photosphere is the visible "surface" of our Sun, a thin layer named after the Greek word for "light." This layer shines brilliantly, radiating the sunlight that illuminates our skies across the entire visible spectrum. In a scientific fashion, the photosphere is a 100 km-thick layer centered around the layer where $\tau_{500} = 1$ (Priest (1982)). Its surface is not smooth but rather textured with a granular pattern when observed at high resolution. These **granules** are dynamic structures caused by the convective motion occurring below the photosphere, where hot plasma rises in bright cells, cools, and sinks at the edges, creating a mosaic of constantly shifting light and shadow. This process is called granulation and it occurs at different size scales ranging from 800 km to 10,000 km. For granules, the temperature varies from 5000 K at the center to 4300 K at the boundary of the granule.

These convective motions are not only responsible for shaping the granules but also play an important role in the generation of MHD waves through the interaction with the magnetic field embedded in the plasma. Motions like twisting and braiding also induce magnetic energy, which is released in the form of magnetic reconnection due to the resistivity of plasma. Both MHD waves and reconnection play important roles in coupling the mechanical energy of the solar interior with the outer atmosphere.

Occasionally, we also observe dark patches emerge on the solar surface, which we call **sunspots**. These are the locations where magnetic fields are highly concentrated, temporarily cooling the plasma below surrounding temperatures and giving it a darker appearance. The region surrounding the sunspot is brighter than the ambient plasma and is called the **plage** region. Collectively, the entire region is called an **active region** and is formed due to the emergence of strong magnetic flux from the convective layer beneath. The strength of the magnetic field in active regions can go up to 7 kG (Siu-Tapia et al. (2019)). These active regions may exist in the form of a pair with opposite polarity of magnetic flux, forming an active-region loop extending into the lower corona, which can be 100,000 km high and 10,000 km wide and have a temperature on the order of a million kelvins. Such loops have an essential role in energy and mass transportation in the solar atmosphere, which causes heating in the

chromosphere and corona.

Overlaying these magnetic and convective features is another fundamental dynamical process: the *p*-mode (pressure-mode) oscillations of the Sun. These are global, acoustic standing waves excited by convective turbulence beneath the photosphere. With typical periods of around five minutes, *p*-modes are confined primarily to the solar interior, trapped between the surface and a depth of roughly 200,000 km. However, their signatures are clearly observable in the photosphere, especially in the quiet sun, as subtle oscillatory motions—both vertical and horizontal—of the solar surface.

The **chromosphere** is the part of the lower atmosphere right above the photosphere and is about 2000 km thick. It is usually invisible to us as it is drowned by the brightness of the photosphere. Still, it can be seen during an annular solar eclipse as a reddish halo around the Moon when it has entirely covered the solar disk. The reddish color is given by **Lyman-alpha emission**, which is prominent in the chromosphere.

The chromospheric structure is highly non-uniform. Its temperature varies from 6000 K at the bottom to a minima of around 4000 K, after which it rises to 25,000 K and eventually reaches a million kelvins in the transition region. Line emissions in the chromosphere are predominantly in UV spectra, which are emitted by elements in their first excited state, mostly Lyman alpha, Mg II and Ca II, indicating a much lower temperature when compared to the corona. For a quantitative determination of the temperature, the energy interplay between emission and absorption needs a detailed study.

Being a dynamic system, we can observe many transient features in the chromosphere. One of the prominent features is the jets of plasma called **spicules**. Spicules are fiery columns that surge upwards with a velocity of around 20 to 30 km/s, reaching heights of about 10,000 km and appear as a transient forest of plasma across the sun.

Based on observations, spicules are categorized into Type I and II. **Type I** spicules are typically found in active regions or quiet Sun areas, often near strong magnetic fields. These spicules exhibit dynamic fibril-like motions and follow characteristic parabolic trajectories. They have velocities ranging between 10 and 40 km/s and lifetimes of approximately 3 to 5 minutes (de Pontieu et al. (2007)). In contrast, **Type II** spicules are known for their more complex dynamics, which include twisting and swaying motions. Type II spicules have a shorter life, lasting about 10 to 150 seconds, but they can achieve significantly higher velocities (de Pontieu et al. (2007)).

Theoretical models of spicule launch include various drivers such as shock waves, Alfvén waves, and magnetic reconnection, but are not well understood because of insufficient resolution and sensitivity of our observations Samanta et al. (2019). A number of numerical studies have explored the mechanisms behind spicule formation, consistently indicating that they result from the leakage of magnetoacoustic oscillations in the chromosphere Heggland et al. (2007).

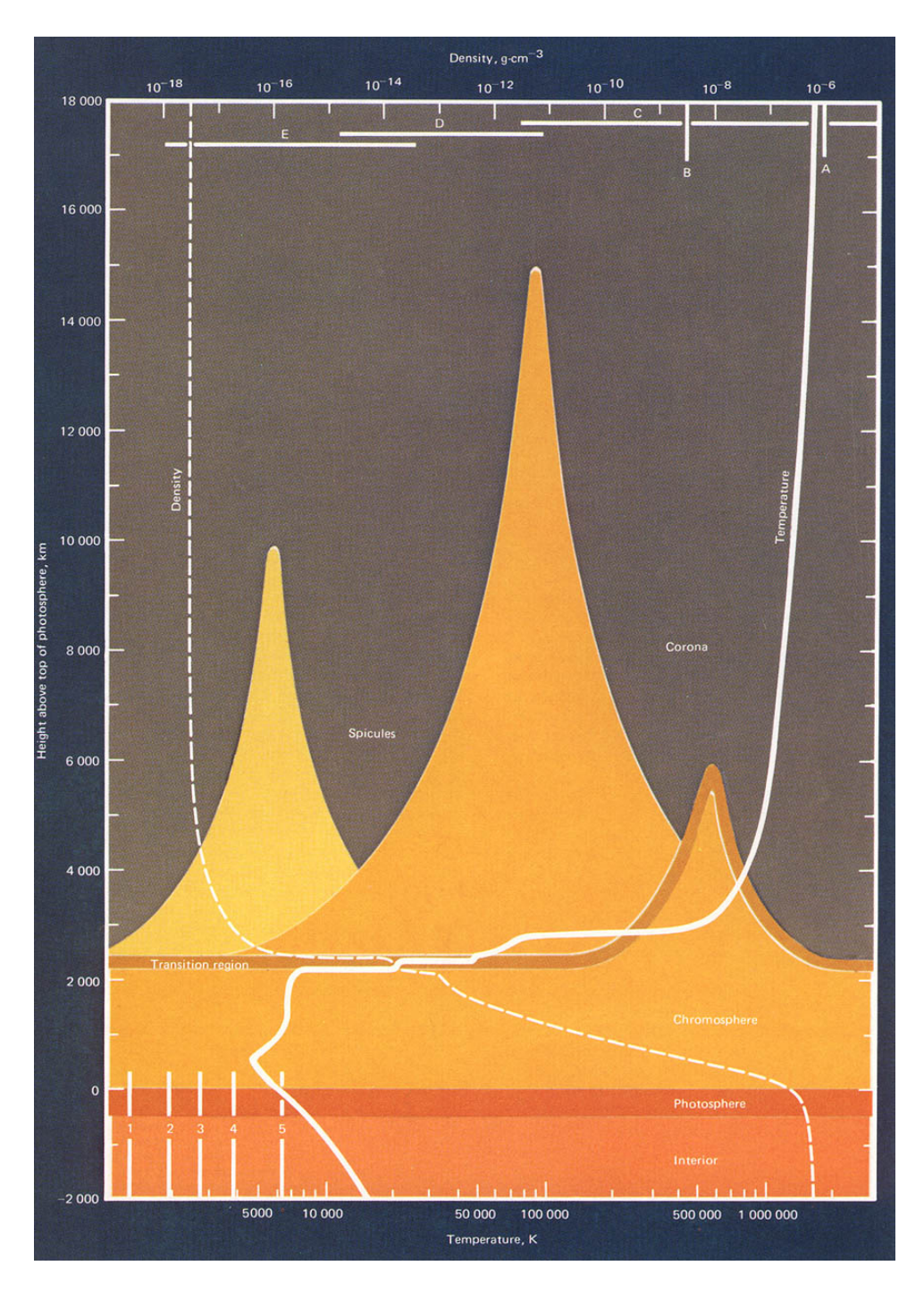


Figure 1.2: This plot illustrates the variation of temperature and density with height in the solar atmosphere. The orange peaks correspond to spicules extending from the chromosphere into the lower corona. The dark yellow band marks the transition region — a narrow layer, only a few hundred kilometers thick, that closely follows the spicule structures. This region serves as a boundary separating the cooler, denser chromosphere from the hotter, more rarefied corona. This image is taken from book *New Sun: The Solar Results From Skylab.* by Eddy and Ise (1979)

An analogy has also been observed between spicules and the forest of polymeric jets generated by subjecting polymeric fluid to the accelerating front of non-linear quasi-periodic waves. In the chromosphere, such acceleration fronts can be generated by the convection of plasma be-

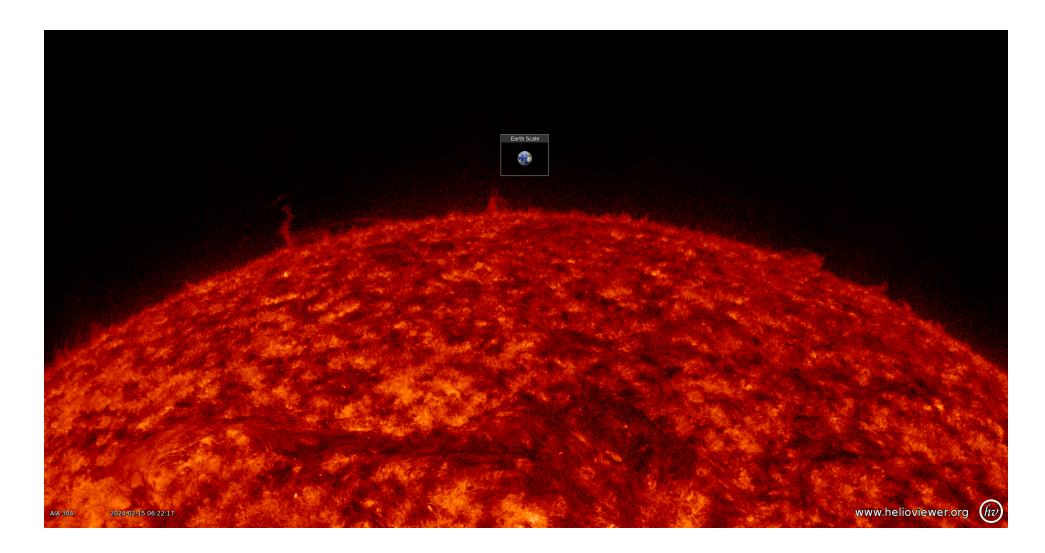


Figure 1.3: Here we can see the transient forest of spicules and they are spread all over the solar surface. Image is taken by SDO AIA on 2024-5-21 in 304nm He II lines. Image of Earth is for scale.

neath the photosphere and magnetic reconnection as well. It is still an open question if such mechanisms are enough to sustain the large number of spicules observed in the chromosphere Dey et al. (2022).

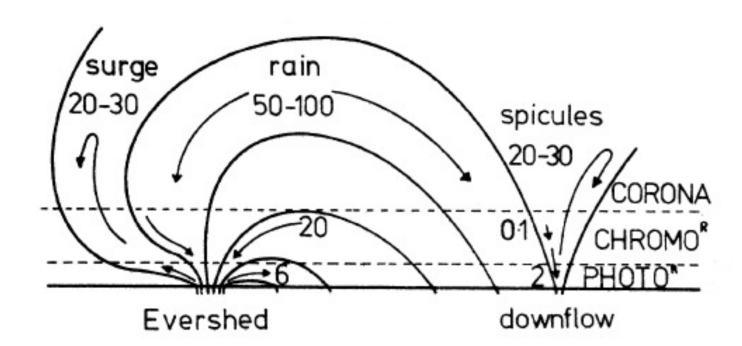


Figure 1.4: Ground-based observations of active-region flows. Image is taken from book *Solar Magnetohydrodynamics* by Priest (2014)

Another transient feature that originates from the chromosphere is surges that are located around the edge of an active region, usually the footpoints of the magnetic flux emergence region. Surges can rise far higher than spicules, up to 200,000km, and last up to 20 minutes. We also see coronal rain, which occurs when plasma inside the coronal loop cools down and falls along the curved path created by magnetic fields.

transition region, which lies above the chromosphere, is a very thin and highly dynamic layer of the solar atmosphere, approximately 100 km thick. The temperature rise in this region is immense, from 30,000 K to 1 MK, which is then sustained throughout the **corona**. The corona is visible as a bright halo extending outward in a streamer-like structure made of plasma

following the sun's magnetic field. Such structures are called **coronal streamers** and extend up to heights of 1 to 10 solar radii.

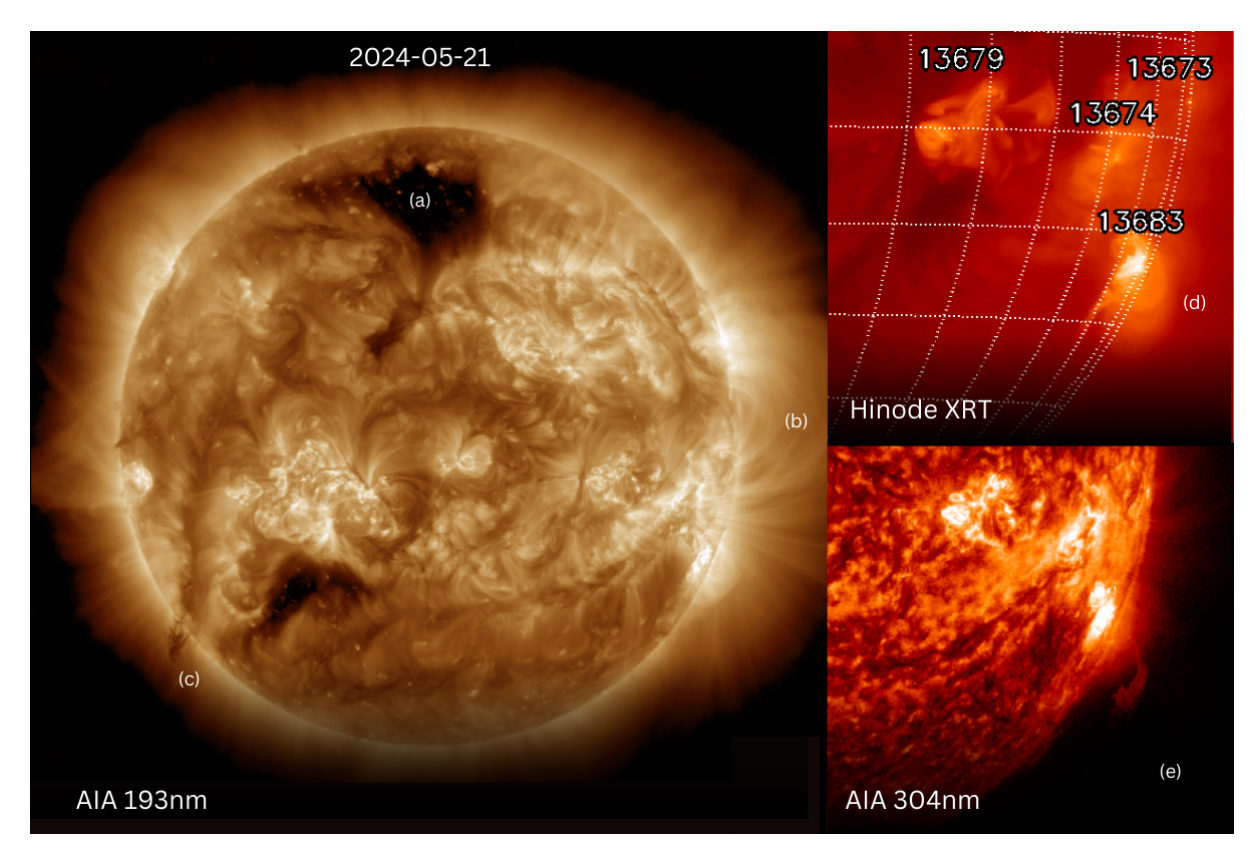


Figure 1.5: Observations taken on 21-5-2-2024 by SDO AIA (Image on the left and bottom right) and Hinode (top right) showing the transient feature of the sun. We can observe (a) a coronal hole, (b) coronal loops, (c) prominence, (d) X-Ray bright points in the XRT image by Hinode, and (e) a filament structure hanging in the corona. Priest (2014)

The corona is observed in soft X-rays, which can only be seen through space-based telescopes as X-rays are absorbed mainly by Earth's atmosphere. In X-ray images, we can observe three coronal features: coronal holes, active regions, and X-ray bright points Priest (2014).

Coronal holes have predominantly open magnetic field lines, forming a highway for plasma to flow outward, resulting in the fast solar wind. In active regions, the magnetic fields form loops due to the bipolar configuration of magnetic fields. Coronal loops are prominently observed in **extreme ultraviolet** (EUV) wavelengths, offering unprecedented details of energetic events happening around them (Liu and Ofman (2014)). These events carry significant energy, which dissipates in the corona, heating it to temperatures of a million kelvins.

These energetic events may have slightly different observational signatures, but they all originate from the twisting and shearing of loop magnetic fields. Due to convective and photospheric motions, magnetic flux emerges from the photosphere, trapping hot plasma within it. When these magnetic field lines reconnect, magnetic potential energy is converted into plasma's thermal and kinetic energy, resulting in a solar flare.

In cases where coronal loops are exceptionally large, magnetic reconnection can push a vast amount of plasma material held within the loops, ejecting it along the field lines. Such ejections of plasma material are known as coronal mass ejections (CMEs).

Besides coronal loops, prominences are another important feature observed in the corona. Prominences are dense, cool plasma structures suspended within the hot corona by magnetic fields. When observed against the sun's disk, they appear as bright filaments, while along the limb, they appear as towering loops. Prominences can remain stable for days or weeks but may become unstable due to magnetic reconnection or external disturbances. When destabilized, they can erupt as part of a CME, ejecting plasma into interplanetary space.

For the most part, solar research focuses on the energy balance of the sun's atmosphere and how such events contribute to such absurd temperatures in the atmosphere, from the photosphere to the corona (Gibson and Fan (2006)). Now, there are two phenomena at work in injecting energy into the atmosphere: global phenomena and local phenomena. Global phenomena are associated with the *p*-mode oscillations, which permeate throughout the solar surface, and it is widely studied how the acoustic and magnetic waves are generated from the *p*-modes and their propagation through the atmosphere, reaching higher heights and possibly dissipating energy into the corona, causing coronal heating. Local phenomena are usually eruptive events that inject large amounts of energy at once and are transported through wave generation and reconnection.

1.3 Coronal heating

Understanding the coronal heating problem requires a detailed examination of how energy is transported and deposited within and among different layers of the solar atmosphere. The energy from the center is transported to the surface through radiative and convective processes. But as this energy reaches the photosphere, energy transport becomes less trivial, particularly in the chromosphere and corona, which become less straightforward.

One of the most promising candidates for this energy transport is **magnetohydrodynamic** (MHD) waves. These waves, which arise from the interplay between magnetic fields and plasma motions, can carry substantial amounts of energy from the lower atmosphere into the corona. Various types of MHD waves, including Alfvén waves and slow and fast magnetoacoustic waves, are believed to be generated in the photosphere and propagate upward along magnetic field lines.

Alfveń waves are capable of transporting energy over large distances without dissipating in the lower atmosphere. But their dissipation in the corona through **phase mixing** or **resonant absorption** can heat the corona, making it a good candidate for coronal heating. However, it is also necessary to acknowledge that coronal heating is not a consequence of waves alone; **mag**-

netic reconnection also plays an equally important role in it. The quest is about understanding to what extent each of these mechanisms heats the corona. Let's take a look at the possible heating mechanisms in the solar atmosphere.

1.3.1 Heating Mechanisms

Heating mechanisms in the solar atmosphere can be classified into two categories based on the influence of magnetic fields. When magnetic fields are significantly involved, it is referred to as a magnetic heating mechanism. If not, then it pertains to hydrodynamic heating.

Energy Carrier	Dissipation Mechanism		
Magnetic Heating Mechanisms			
1. Direct Current (DC) Mechanisms			
Current sheets	Reconnection (turbulent heating, wave heating)		
2. Alternating Current (AC) or Wave Mechanisms			
Alfvén waves (transverse, torsional)	Mode coupling, resonance heating, phase mixing,		
	compressional viscous heating, turbulent heating,		
	Landau damping, RA		
Slow MHD waves	Shock damping, resonant absorption		
Longitudinal MHD tube waves	Shock damping, resonant absorption		
Fast MHD waves	Landau damping		
Hydrodynamic Heating Mechanisms			
Acoustic waves (P $<$ $P_{\text{acoustic cut-off}}$)	Shock dissipation		
Pulsational waves (P > $P_{\text{acoustic cut-off}}$)	Shock dissipation		

Table 1.1: Summary of heating mechanisms by Ulmschneider (1998)

The interplay between plasma and magnetic fields fundamentally governs the dynamics of the solar atmosphere. This interaction is encapsulated in the induction equation of magnetohydrodynamics (MHD):

$$\frac{\partial \mathbf{B}}{\partial t} = \nabla \times (\mathbf{v} \times \mathbf{B}) + \eta \nabla^2 \mathbf{B}, \tag{1.1}$$

where **B** is the magnetic field, **v** is the plasma velocity, and η is the magnetic diffusivity. In the ideal MHD limit ($\eta = 0$), the magnetic field lines are said to be *frozen-in* to the plasma, implying that perturbations in plasma motion directly perturb the magnetic field and vice versa.

A critical parameter in determining the behavior of plasma and magnetic fields is the **plasma-\beta**, the ratio of thermal pressure to magnetic pressure. The plasma- β in the solar atmosphere exhibits strong height dependence as shown in Fig 1.9. Thermal pressure dominates in

the photosphere and lower chromosphere, where $\beta \gtrsim 1$, and convective motions can deform or drag magnetic field lines. However, magnetic forces overwhelmingly control plasma dynamics as we ascend into the upper chromosphere, transition region, and corona, $\beta \ll 1$. This shift plays a key role in generating and propagating **MHD waves**, now widely recognized as critical carriers of energy from the lower atmosphere into the corona.

MHD Waves and Coronal Heating Mechanisms

Photospheric convection acts as a continuous driver of a broad spectrum of MHD waves, including **Alfvén waves**, **fast magnetoacoustic waves**, and **slow magnetoacoustic waves**. These waves are excited via buffeting of magnetic flux tubes, vortex motions, or *p*-mode leakage and can propagate along magnetic field lines into the upper atmosphere. Their role in heating the solar corona is typically categorized into two broad mechanisms:

- AC Heating (Wave Dissipation): When the characteristic timescale of the photospheric driver is shorter than the Alfvén transit time ($t \ll t_A$), the perturbations generate propagating MHD waves. As these waves move upward, they can undergo various nonlinear interactions—such as **phase mixing**, **resonant absorption**, and **mode conversion**—which lead to deposition of localized energy and plasma heating.
- DC Heating (Field-Line Braiding): If the footpoint motions evolve on a slower timescale than the Alfvén transit time $(t \gg t_A)$, magnetic stresses build up as field lines become twisted and braided. Energy is stored in these stressed configurations and is eventually released through magnetic reconnection events that convert magnetic energy into heat and bulk plasma motions.

While these two paradigms are distinct in terms of the temporal characteristics of the drivers and dissipation mechanisms, they share common ground. Both assume that the primary energy input originates from photospheric or chromospheric motions and fine-scale structuring of the magnetic field (e.g., flux tubes, current sheets) becomes crucial for efficient energy dissipation (Gomez et al. (2000)).

1.4 Solar Oscillations

Stars, including our Sun, are dynamic systems governed by the tapestry of several forces—pressure, gravity, magnetic fields, and rotation. These forces consistently maintain the equilibrium, but disturbances such as fluctuations in local temperature or pressure can displace the system. In response, the restoring forces attempt to return the medium to equilibrium, giving rise to waves that propagate throughout the stellar material.

At first glance, one might expect such stellar motions to be chaotic and featureless, akin to the boiling of water. Motions would appear random, so the resulting velocity and pressure fields would be described statistically, leading to a continuous spectrum of noise across all frequencies and wavelengths.

However, observations (such as Leighton et al. (1962)) reveal a more structured feature instead of random turbulence. Stars exhibit oscillations at specific frequencies creating a well-defined patterns indicating certain **modes** in action. Modes are the standing waves which arise when waves are trapped in a cavity interacting with itself. The boundary conditions of this cavity lead to a discrete set of allowable solutions to the wave equation, each corresponding to a specific **eigenfrequency**.

In stars, one like our Sun, resonant cavity is established by the sharp density gradient in the outer layers. The excitation of modes is said to be stochastic in origin, driven by the convective motion beneath the photosphere. These convective motions act as a broadband source, exciting a wide range of frequencies, but only the natural eigenfrequencies of the solar cavity result in standing waves with significant amplitudes.

These resonant oscillations are not just mathematical curiosities—they serve as powerful tools in **solar** and **stellar seismology**. By observing the surface signatures of these modes, we can infer the physical conditions deep inside a star, far beyond direct observational reach.

Each oscillation mode corresponds to a particular restoring force and spatial structure. The main classes of modes include:

- *p*-modes (pressure modes): Oscillations where pressure acts as the primary restoring force. These modes dominate in the outer convective zone and are sensitive to sound-speed profiles.
- **g-modes** (**gravity modes**): Oscillations driven by buoyancy, prevalent in stably stratified regions such as the radiative interior. These modes are particularly valuable for probing deep solar layers.
- **f-modes** (**fundamental or surface gravity modes**): Surface-confined modes that behave like gravity waves at the interface between two fluids, with no radial nodes.

The detection of such modes through **helioseismology** (for the Sun) or **asteroseismology** (for other stars) allows astronomers to probe stellar interiors indirectly.

In a stratified stellar atmosphere, where the density decreases significantly with height, wave behavior becomes complex. One major effect of this density stratification is varying amplitude with height. Specifically, if a wave carries energy upward without being refracted, its energy flux remains constant. However, since density drops with height, the wave's velocity amplitude must increase to maintain that constant energy flux.

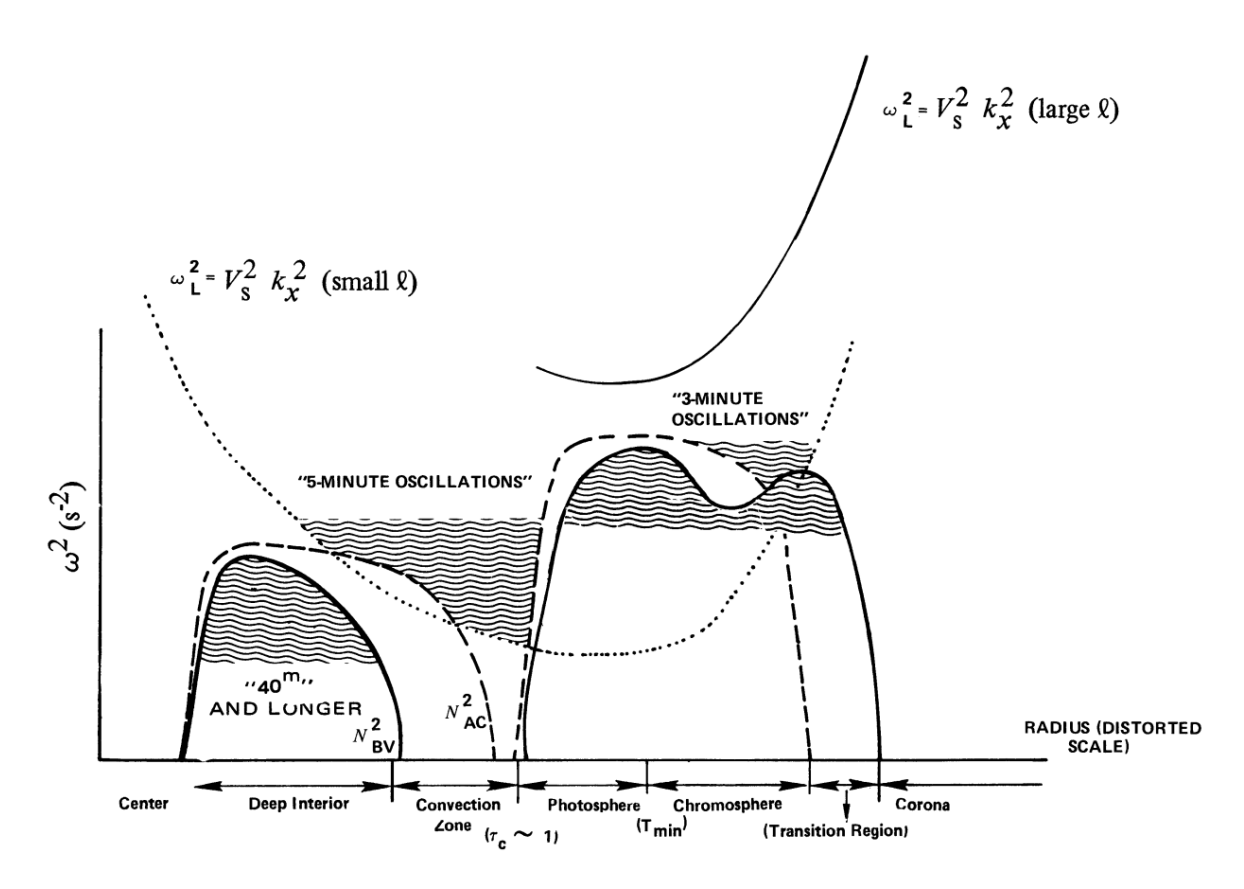


Figure 1.6: Wave propagation diagram for the sun. X-axis represents the radial distance distorted to emphasize different layers. Solid line represents the Brunt-Väsälä buoyancy frequency, dashed line represents the cut-off frequency and dotted line is the dispersion relation for waves in spherical geometry as of in stars (Leibacher and Stein (1981)). This diagram represents the types of waves trapped in different resonant cavities in the Sun. In the interior of the Sun, g-modes are trapped with theoretical time period of 40 minutes. Near the solar surface, *p*-modes of 5-minute time period is trapped and in chromosphere 3-minute oscillations are trapped.

Mathematically, the velocity amplitude scales inversely with the square root of the density, approximately as (Leibacher and Stein (1981))

velocity amplitude
$$\propto \rho^{-1/2} \propto e^{z/2H}$$
, (1.2)

where H is the scale height, a measure of how quickly the density drops off in the atmosphere. Thus, as one ascends in a star's atmosphere, the same wave appears amplified.

Another important consequence of stratification is the appearance of a low-frequency cutoff for acoustic waves. If a disturbance oscillates too slowly, pressure differences that would normally drive sound waves do not have enough time to build up. This occurs because sound waves propagate rapidly and can re-establish pressure equilibrium before the stellar gas parcel has time to move significantly. Frequency for the cutoff is determined by,

$$v_c = \frac{c_s}{4\pi H} \tag{1.3}$$

Where γ is the adiabatic coefficient and $c_s = \sqrt{\gamma gH}$ is the speed of sound and H is the density

scale height (Lamb (1909)). The density scale height describes the distance over which the density (or pressure) decreases by a factor of e and is given by,

$$H = -\left(\frac{1}{\rho} \frac{d\rho}{dy}\right)^{-1} \tag{1.4}$$

For ideal gas, we will have,

$$H = \frac{K_B T}{\mu mg} \tag{1.5}$$

As long as we consider a non-magnetic atmosphere, any acoustic wave having a wavelength longer than the density scale height will get evanescent, i.e., it will decay and won't reach higher heights. But when we consider the magnetic fields as well, the nature of waves also changes. In the regions of strong magnetic fields such as sunspots, inter-granular region, plages, and arcades, acoustic waves undergo wave mode conversions, i.e., the acoustic waves are converted into magnetic waves. Many studies have shown that the inclination of the magnetic field with respect to the axis of stratification leaks out *p*-mode into the chromosphere and corona De Pontieu et al. (2004); Rajaguru et al. (2019). Before getting into the wave propagation in the solar atmosphere, let's delve deeper into the magneto-hydrodynamic waves to understand the different modes excited when plasma is mechanically excited.

1.4.1 *p*-mode oscillations

p-modes have been one of the most prominent and well-studied features of solar oscillations. These oscillations are characterized by pressure as the dominant restoring force and are responsible for the Sun's famous **5-minute oscillations**. These modes are trappedheat in an acoustic cavity bounded from below by increasing sound speed in the solar interior and from above by the rapid drop in density near the photosphere, which acts as a partial reflector.

Historically, the nature of the 5-minute oscillations has been a topic of active discussion. It was first observed by Leighton et al. (1962) and the explanation for it was first proposed by Ulrich (1970). It was suggested that these oscillations arise due to acoustic waves generated by turbulent convection in the Sun's outer layers. The sound speed increases with depth, proportional to the square root of temperature, causing acoustic waves to refract inward. This sets a lower turning point where the wave is reflected back upward. The upper turning point lies near the solar surface, where a steep density gradient leads to partial reflection. Together, these boundaries form a resonant cavity in which standing acoustic modes can develop.

These p-modes are not only vital for helioseismology but also serves to our understanding of wave physics in a stratified magnetic plasma. Now we shall focus on how p-mode oscillations interact with solar atmosphere and its role in energy transport. For that we have to delve a bit deeper into the magneto-hydrodynamic waves.

1.5 Magneto-hydrodynamic Waves

Waves in the solar atmosphere are often known as magneto-acoustic waves or magneto-hydrodynamic (MHD) waves. Such waves are governed by following equations,

$$\frac{\partial \rho}{\partial t} + \vec{\nabla} \cdot (\rho \vec{v}) = 0 \tag{1.6}$$

$$\rho \frac{\partial \vec{v}}{\partial t} = -\vec{\nabla}p + \frac{1}{\mu_0} (\vec{\nabla} \times \vec{B}) \times \vec{B} - \rho g \hat{z}$$
(1.7)

$$\frac{\partial}{\partial t} \left(\frac{p}{\rho^{\gamma}} \right) = 0 \tag{1.8}$$

$$\frac{\partial \vec{B}}{\partial t} = \vec{\nabla} \times (\vec{v} \times \vec{B}) \tag{1.9}$$

$$\vec{\nabla} \cdot \vec{B} = 0 \tag{1.10}$$

The resulting temperature follows from:

$$T = \frac{mp}{k_B \rho} \tag{1.11}$$

Now, to study its behaviour, we must disturb our system. For that, we decompose each variable into a static equilibrium background (subscript 0) and a small perturbation (subscript 1):

$$\rho = \rho_0 + \rho_1$$

$$\vec{v} = \vec{v}_1$$

$$p = p_0 + p_1$$

$$\vec{B} = \vec{B}_0 + \vec{B}_1$$

Assumptions:

- The background fields ho_0, p_0, \vec{B}_0 are time-independent.
- Background velocity is zero ($\vec{v}_0 = 0$).
- Perturbations $\rho_1, \vec{v}_1, p_1, \vec{B}_1$ are small (linear theory).

The linearized equations for a perturbed magnetized plasma system are:

$$\frac{\partial p_1}{\partial t} + (\vec{v}_1 \cdot \vec{\nabla})p_0 + p_0(\vec{\nabla} \cdot \vec{v}_1) = 0$$
(1.12)

$$\rho_0 \frac{\partial \vec{v}_1}{\partial t} = -\vec{\nabla} p_1 + \frac{1}{u_0} (\vec{\nabla} \times \vec{B}_1) \times \vec{B}_0 - \rho_1 g \vec{\hat{z}}$$

$$\tag{1.13}$$

$$\frac{\partial p_1}{\partial t} + (\vec{v}_1 \cdot \vec{\nabla}) p_0 - c_s^2 \left(\frac{\partial \rho_1}{\partial t} + (\vec{v}_1 \cdot \vec{\nabla}) \rho_0 \right) = 0 \tag{1.14}$$

$$\frac{\partial \vec{B}_1}{\partial t} = \vec{\nabla} \times (\vec{v}_1 \times \vec{B}_0) \tag{1.15}$$

$$\vec{\nabla} \cdot \vec{B}_1 = 0 \tag{1.16}$$

where

$$c_s^2 = \gamma \frac{p_0}{\rho_0} = \gamma \frac{k_B T_0}{m} \tag{1.17}$$

The linearized equations describe how small perturbations evolve in a magnetized, stratified plasma. If we differentiate eq (1.13) w.r.t. time and replace other derivative terms from other equations, we get a single differential equation for velocity perturbation $\vec{v_1}$,

$$\frac{\partial^2 \vec{v}_1}{\partial t^2} = c_s^2 \vec{\nabla} (\vec{\nabla} \cdot \vec{v}_1) - (\gamma - 1) gz(\vec{\nabla} \cdot \vec{v}_1) - g\vec{\nabla} v_{1z} + \frac{1}{\rho_0 \mu_0} \left[\vec{\nabla} \times (\vec{v}_1 \times \vec{B}_0) \right] \times \vec{B}_0 \quad (1.18)$$

For the sake of simplicity, let's consider g = 0 for now, so we have,

$$\frac{\partial^2 \vec{v}_1}{\partial t^2} = c_s^2 \vec{\nabla} (\vec{\nabla} \cdot \vec{v}_1) + \frac{1}{\rho_0 \mu_0} \left[\vec{\nabla} \times \left(\vec{\nabla} \times (\vec{v}_1 \times \vec{B}_0) \right) \right] \times \vec{B}_0$$
 (1.19)

Now, let's assume the solution for v_1 be of the form,

$$\vec{v}_1(\vec{r},t) = \vec{v}_1 e^{i(\vec{k}.\vec{r} - \omega t)} \tag{1.20}$$

So we end up with,

$$\omega^2 \vec{v}_1 = c_s^2 \vec{k} (\vec{k} \cdot \vec{v}_1) + \frac{1}{\rho_0 \mu_0} \left[\vec{k} \times \left(\vec{k} \times (\vec{v}_1 \times \vec{B}_0) \right) \right] \times \vec{B}_0$$
 (1.21)

For further simplicity, let us choose Cartesian axes such that the magnetic field is in \hat{z} direction and \vec{k} makes an angle θ with \vec{B} such that,

$$\vec{k} = k\sin\theta \,\hat{\mathbf{y}} + k\cos\theta \,\hat{\mathbf{z}} \tag{1.22}$$

Let the velocity components be,

$$\vec{v_1} = v_{1x}\hat{x} + v_{1y}\hat{y} + v_{1z}\hat{z} \tag{1.23}$$

and also,

$$V_A = \frac{B_0}{\sqrt{\rho_0 \mu_0}} \tag{1.24}$$

This is analogous to sound speed and popularly known as the Alfvén speed. Now, by expanding all the terms we get,

$$(\omega^2 - k^2 V_A^2 \cos^2 \theta) v_{1x} = 0 (1.25)$$

$$(\omega^{2} - k^{2} \sin^{2}\theta c_{s}^{2} - k^{2} V_{A}^{2}) v_{y} - k^{2} c_{s}^{2} \sin\theta \cos\theta v_{1z} = 0$$
(1.26)

$$-k^{2}c_{s}^{2}\sin\theta\cos\theta v_{1y} + (\omega^{2} - k^{2}c_{s}^{2}\cos^{2}\theta)v_{1z} = 0$$
 (1.27)

To get a non-trivial solution $\vec{v_1} \neq 0$, we require,

$$\det \begin{bmatrix} \omega^{2} - k^{2} \cos^{2} \theta \, v_{A}^{2} & 0 & 0\\ 0 & \omega^{2} - k^{2} \sin^{2} \theta \, c_{s}^{2} - k^{2} v_{A}^{2} & -k^{2} \sin \theta \cos \theta \, c_{s}^{2}\\ 0 & -k^{2} \sin \theta \cos \theta \, c_{s}^{2} & \omega^{2} - k^{2} \cos^{2} \theta \, c_{s}^{2} \end{bmatrix} = 0$$
 (1.28)

Equation (1.28) reduces to the dispersion relation for MHD waves:

$$\left(\omega^{2} - k^{2}\cos^{2}\theta v_{A}^{2}\right)\left[\omega^{4} - k^{2}(c_{s}^{2} + v_{A}^{2})\omega^{2} + k^{4}\cos^{2}\theta c_{s}^{2}v_{A}^{2}\right] = 0$$
(1.29)

Now we have three solutions for this equation,

$$\omega_A^2 = k^2 V_A^2 \cos^2 \theta \tag{1.30}$$

$$\omega_{\pm}^{2} = \frac{k^{2}}{2}(c_{s}^{2} + v_{A}^{2}) \pm \frac{1}{2} \left[(c_{s}^{2} + v_{A}^{2})^{2} - 4c_{s}^{2}v_{A}^{2}cos^{2}\theta \right]^{1/2}$$
(1.31)

Where ω_A is the solution for the Alfvén wave, which is transverse in nature, and ω_{\pm} is longitudinal in nature with two modes: fast MHD wave (ω_+) and slow MHD wave (ω_-). In terms of plasma- β , which (under isothermal conditions) is defined as,

$$\beta = \frac{c_s^2}{v_A^2} = \frac{2nK_BT}{nm_i} \frac{4\pi\rho}{\mathbf{B}^2} = \frac{nK_BT}{\mathbf{B}^2/8\pi} = \frac{Thermal\, Pressure}{Magnetic\, Pressure}.$$
 (1.32)

Our dispersion relation becomes,

$$\frac{\omega_{\pm}^2}{k^2 V_A^2} = \frac{1+\beta}{2} \pm \frac{1}{2} \left[(1+\beta)^2 - 4\beta \cos^2 \theta \right]^{1/2}$$
 (1.33)

The plot for three solutions ($\omega^2/k^2V_A^2$ vs angle θ) for different values of c_s/v_A is given below,

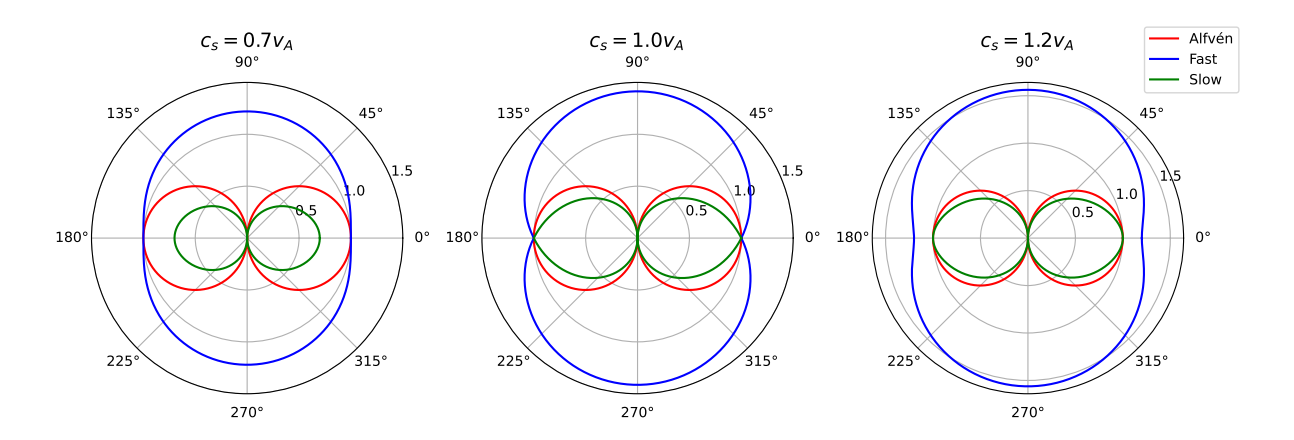


Figure 1.7: Plot for phase velocity (relative to v_A) vs angle for slow, fast and Alfvén mode for a system where $v_A = 0.7c_s$, $v_A = c_s$ and $v_A = 1.2c_s$

Note: Plasma Beta in Adiabatic Condition

In an adiabatic plasma where $c_s^2 = \gamma p/\rho$, the plasma beta becomes:

$$\beta = \frac{p}{B^2/8\pi} = \frac{2(\gamma p/\rho)}{\gamma (B^2/4\pi\rho)} = \frac{2}{\gamma} \frac{c_s^2}{v_A^2}$$

All three magnetohydrodynamic wave modes—Alfvén, slow, and fast—have real solutions, indicating that they exhibit purely oscillatory behavior without any growth or decay. The **fast magnetoacoustic wave** propagates with a velocity greater than both the sound speed and the Alfvén speed, and it typically travels perpendicular to the magnetic field lines. In contrast, the **slow magnetoacoustic wave** travels along the magnetic field direction with a velocity lower than both the sound speed and the Alfvén speed. These distinct propagation characteristics are crucial for identifying wave modes and understanding energy transport in magnetized plasmas.

The behavior of magnetoacoustic (fast and slow) waves—depends strongly on the local **plasma-** β , the ratio of thermal pressure to magnetic pressure. This parameter controls the dominant **restoring force** and the preferred direction of wave propagation. The Table 1.2 summarizes the qualitative nature of slow and fast modes in both low- β ($v_A \gg c_s$) and high- β ($c_s \gg v_A$) environments, which commonly occur in different regions of the solar atmosphere. Understanding this distinction is essential for interpreting wave dynamics and mode conversion processes in structured magnetized plasmas.

Having understood the behavior of acoustic (*p*-mode) pulsations in the solar interior, the next natural question arises: what happens when these waves approach the solar atmosphere? Do they penetrate into the outer layers, or are they reflected back? More importantly, if they do reach higher altitudes, is their energy dissipated or transformed into other modes of motion that could potentially contribute to heating?

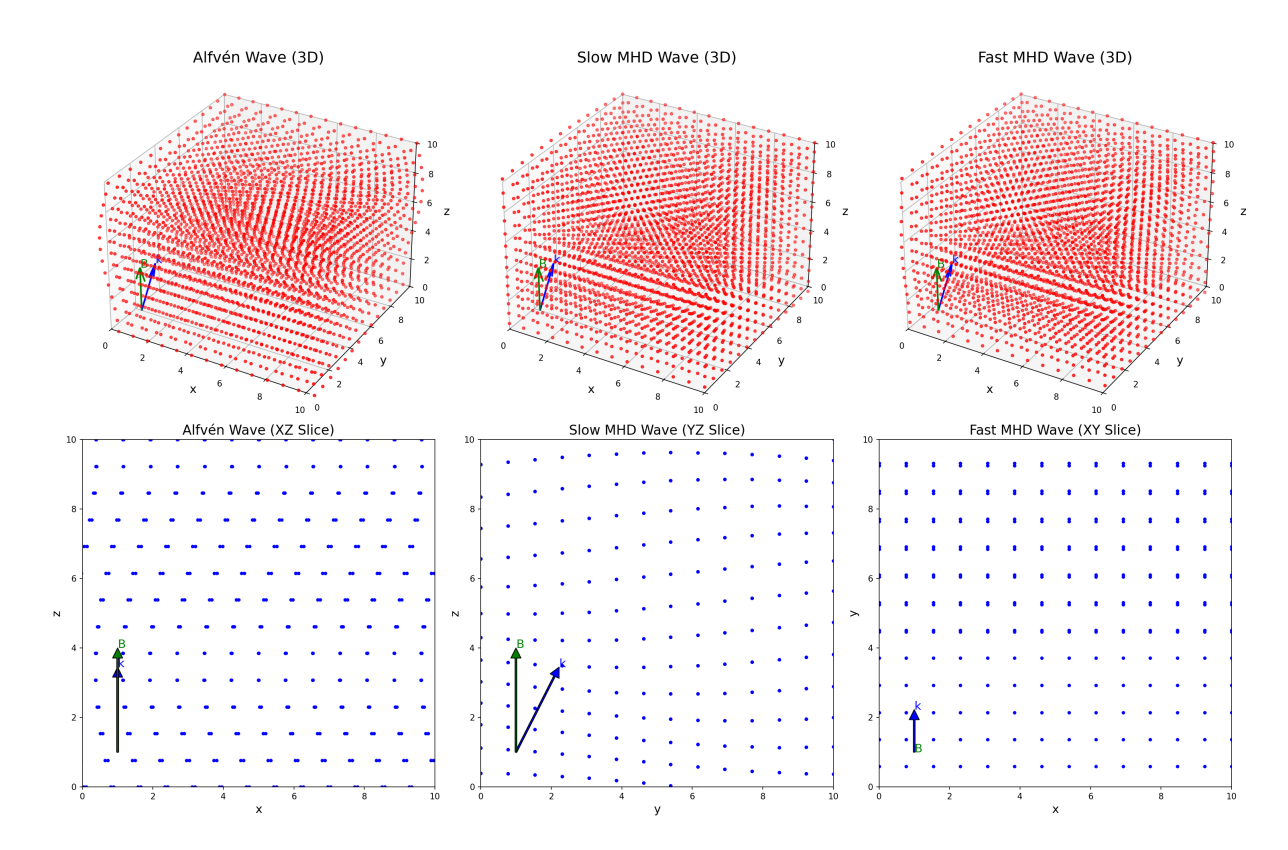


Figure 1.8: How particles oscillate in different modes of MHD waves in 3D, along with their 2D slices to understand the motion of particles better. Vectors represent the direction magnetic field and wave propagation.

Table 1.2: Nature of slow and fast MHD modes in different plasma- β regimes.

Wave Mode Low β ($c_s \ll v_A$)		High β $(c_s \gg v_A)$
Fast mode	Magnetic in nature	Acoustic in nature
rast mode	(restored mainly by magnetic tension)	(restored mainly by pressure gradients)
Slow mode	Acoustic in nature	Magnetic in nature
Slow mode	(restored mainly by pressure gradients)	(restored mainly by magnetic tension)

1.5.1 Mode Conversion in the Solar Atmosphere

Mode conversion is a fundamental mechanism that governs how wave energy is redistributed as it traverses regions of varying plasma properties. With stratification and complex magnetic topology in solar atmosphere, mode conversions are pivotal for transferring energy between different wave modes—magnetoacoustic, and Alfvénic—and thereby influence energy transport and dynamics across layers. A key region where this transformation occurs is the Alfvénacoustic equipartition layer, where the sound speed c_s equals the Alfvén speed v_A . At this layer, waves can undergo mode conversion, a process by which wave energy is redistributed among the available MHD modes. The efficiency and nature of this conversion depend sensitively on the angle between the wavevector \vec{k} and the magnetic field \vec{B} .

However, there is a lack of consensus in the literature regarding the terminology of mode

conversion. As described by Cally (2006), mode conversion may either refer to a change in the wave mode (e.g., from slow to fast magnetoacoustic mode or vice versa), or a change in the nature of the restoring force (e.g., from acoustic-dominated to magnetic-dominated slow mode) as described in Khomenko et al. (2008). So, we have two kinds of conversion we need to consider.

In two-dimensional (2D) models, fast-to-slow conversion is strongest for magnetic field inclinations around 20° – 30° from the vertical. This condition is commonly found in so-called magnetoacoustic portals (Jefferies et al. (2006)), which efficiently couple subphotospheric *p*-mode oscillations to atmospheric magnetoacoustic waves (Cally and Goossens (2008); Khomenko et al. (2008)).

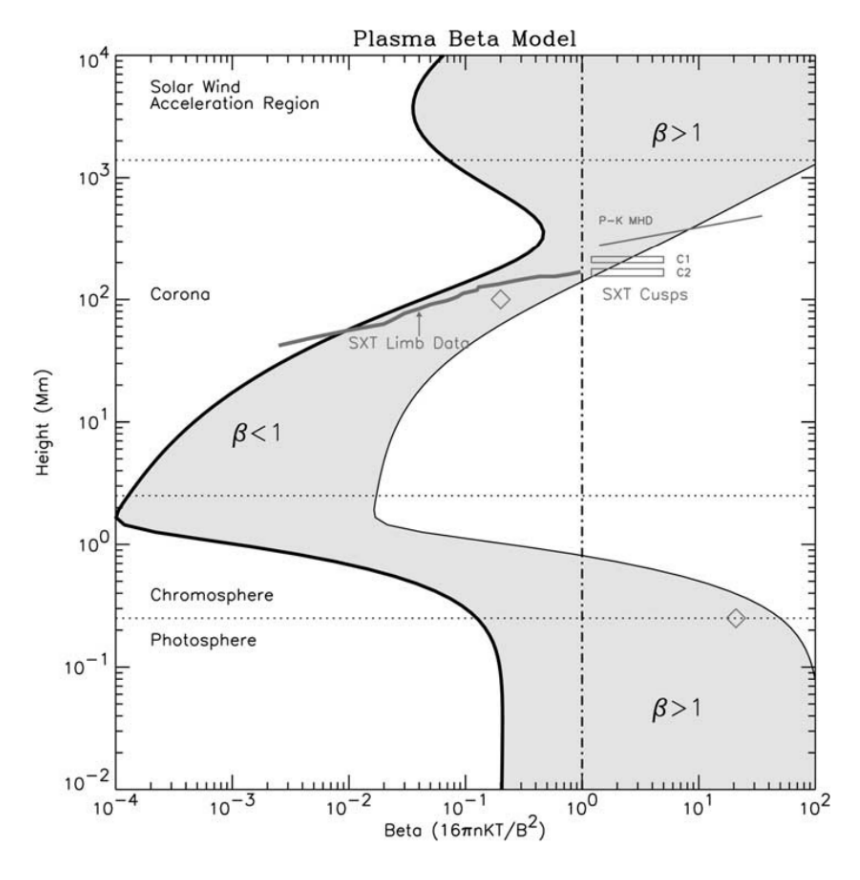


Figure 1.9: Plasma beta profile over an active region of the sun. The plasma beta is shown as the shaded region Gary (2001)

Beyond the reflection height of fast waves, with $\omega \approx v_A k_h$ (with ω the wave frequency and k_h the horizontal wavenumber)—we have fast-to-Alfvén mode conversion. This conversion is inherently a **three-dimensional (3D) phenomenon**, where **non-coplanarity** between the wave propagation direction and the magnetic field becomes necessary. Cally and Hansen (2011a) demonstrated that Alfvén waves can be generated in the low chromosphere from fast magnetoacoustic waves beyond their reflection point, even in the absence of direct photospheric drivers.

Thus, mode conversion serves not only as a source of new wave types but also a mechanism for energy redirection. Accurate modeling of these processes requires fully 3D simulations or at least 2.5D models, which have dependence in all three coordinates, along with careful consideration of magnetic geometry, nature of wave driver, and atmospheric stratification.

1.5.2 Interaction with jets

Solar jets are the plasma ejections that occur in the solar atmosphere, typically extending from the chromosphere into the corona. Interaction between global solar oscillations and such transient events has also become crucial in understanding the mode conversion and energy transport in chromosphere and corona. Recent studies like Skirvin et al. (2023) have demonstrated that **small-scale solar jets**, including spicules and fibrils, play a vital role in energy transport in the lower solar atmosphere. Several observations have found that jets can excite MHD waves, including **high-frequency transverse oscillations**, and hence carry substantial energy flux in the chromosphere and corona (Okamoto and De Pontieu (2011); Srivastava et al. (2017)). Observations suggest these oscillations have a time period of 20-50s, which is significantly smaller than the time period of the granular motion (300-1000s, Schrijver et al. (1997)). A study by Kuniyoshi et al. (2024a) suggested that *p*-mode interaction indeed play an important role in generating such high-frequency spicule oscillations.

1.6 Previous works

Over the past two decades, observations of the solar atmosphere have revealed a diverse and dynamic spectrum of wave phenomena. Instruments like the *Solar Optical Telescope (SOT)* aboard *Hinode* and the *Coronal Multi-Channel Polarimeter (CoMP)* have provided unambiguous evidence for the presence of **ubiquitous Alfvénic oscillations** in both the chromosphere and corona De Pontieu et al. (2007); Tomczyk et al. (2007). These transverse oscillations, peaking around ~3–4 mHz, exhibit a frequency range closely tied to the Sun's internal *p*-mode oscillations, hinting at a profound coupling between the solar interior and its outer atmosphere. However, the precise nature of these waves—whether pure Alfvén or kink modes—depends intricately on the magnetic and density structuring of the medium, which evolves with height Van Doorsselaere et al. (2008). This makes sunspot atmospheres, with their more coherent magnetic topology, particularly favorable environments for the propagation of Alfvénic modes.

From the observations made by Helioseismic and Magnetic Imager (HMI) and the Atmospheric Imaging Assembly (AIA) on board NASA's Solar Dynamics Observatory (SDO), a study by Rajaguru et al. (2019) examined how the properties of the magnetic field, specifically its inclination and strength, influence the propagation of acoustic waves in the solar atmosphere.

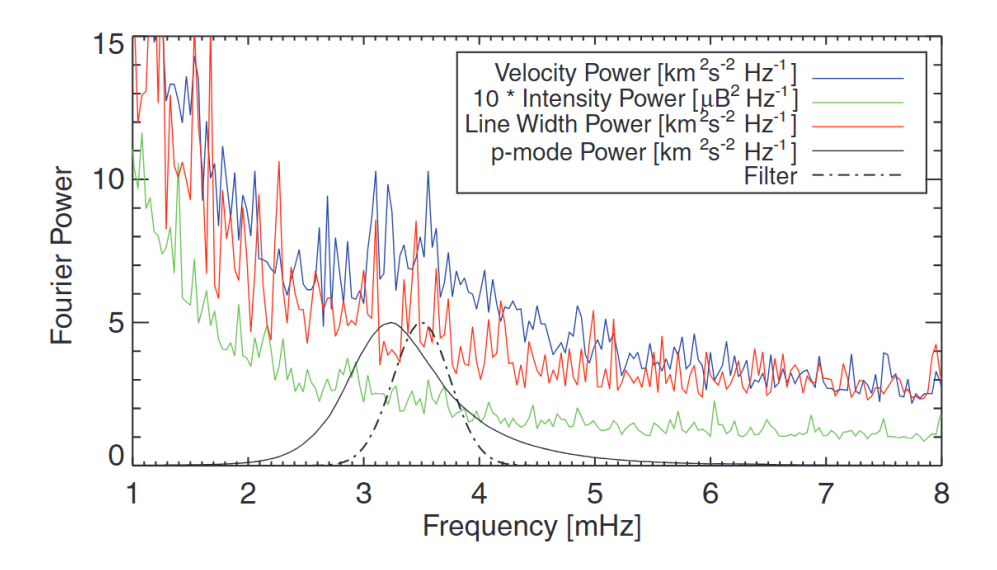


Figure 1.10: The Fourier power spectrum for Doppler velocity (blue), intensity (green), and line width (red) as measured by the COMP instrument. The Doppler velocity spectrum clearly shows a strong and broad peak around 3.5 mHz, indicating dominant oscillations at this frequency. Tomczyk et al. (2007)

The observations reveal that the acoustic energy flux in the 2–5 mHz frequency range from the upper photosphere to the lower chromosphere.

This observation echoes with the theoretical proposal by De Pontieu et al. (2004), who argued that the inclination of the magnetic field can significantly reduce the effective acoustic cutoff frequency. In inclined magnetic flux tubes, the effective gravity is reduced by $\cos\theta$, which leads to a higher cutoff period. This facilitates the tunneling of wave energy into the chromosphere even when the waves are technically non-propagating (evanescent) in the photosphere.

In a fairly recent observation study conducted by Morton et al. (2025) found frequencies higher than 20 mHz in corona, but the significant energy is carried by waves with frequencies between 3-20 mHz. But they also suggested that dissipating energy fromm low frequency waves can't take place directly because they don't generate strong gradients for dissipation to occur efficiently. Turblence might play important role by cascading energy to smaller scales but it is still not known if waves experience turbulence at all and if they do, how fast and how often such process occurs.

These observations highlight the significance of *p*-modes and their implications for coronal heating and solar wind acceleration — both longstanding problems in solar physics. Numerical and theoretical studies (e.g., Cranmer and van Ballegooijen (2005)) have shown that Alfvén waves generated at or below the photosphere can propagate upward and deposit energy through dissipation processes in the corona. More recently, it has been proposed that these waves need not all originate from direct excitation at the surface; rather, they may arise via **mode conversion from fast magnetoacoustic waves** in the **low chromosphere** Cally and Hansen (2011b).

The **fast-to-slow conversion** at the $\beta \approx 1$ layer has been well documented in 2D simulations and theory, particularly for inclined fields which act as *magnetoacoustic portals* linking subphotospheric oscillations to the atmosphere Jefferies et al. (2006). However, the **fast-to-Alfvén conversion**, which occurs above the **fast wave reflection height** $z_{\text{ref}} \sim \omega/(k_h v_A)$, becomes increasingly dominant in 3D settings at chromospheric and coronal heights, allowing energy to leak into the upper atmosphere as Alfvénic flux Cally and Goossens (2008); Newington and Cally (2010). Importantly, this flux can, under certain configurations, exceed the acoustic contribution, especially in low- β regions with inclined magnetic fields.

Thus, understanding how these waves propagate, reflect, convert, and ultimately **dissipate** across the β transition zones is essential for constructing a consistent picture of solar atmospheric energetics. It also underscores the need for detailed **3D modeling and analysis**, as well as refined diagnostics from observations, to fully unravel the multiscale coupling between the **solar interior**, **atmosphere**, **and heliosphere**.

Alfvén wave dynamics in structured solar atmospheres—such as those found in sunspots and magnetic flux tubes—have been the focus of numerous numerical and theoretical investigations. In particular, the conversion of fast magnetoacoustic waves into Alfvén waves and their subsequent propagation or reflection due to gradients in the Alfvén speed have received substantial attention. It is well-established that p-modes, driven by convective motions below the photosphere, can undergo mode conversion as they interact with magnetic structures in the solar atmosphere. Theoretical and numerical investigations, such as those by Cally and Goossens (2008) and Khomenko and Cally (2012), have demonstrated that p-modes—initially fast acoustic waves—can convert into fast magnetoacoustic waves near the equipartition layer (where $c_s = v_A$), and subsequently into Alfvén waves in the low- β upper atmosphere. The efficiency of this double mode conversion process is highly sensitive to magnetic field inclination, horizontal wavenumber, and azimuthal angle Cally and Hansen (2011a).

Observationally, enhancements in coronal Alfvénic wave power near 4 mHz have suggested a possible link with the \sim 3 mHz p-mode spectrum, implying a coupling between these wave modes Morton et al. (2019); Hansen and Cally (2012). Simulations by Kuniyoshi et al. (2024b) and Gao et al. (2023) have attempted to reproduce this behavior using p-mode drivers in various magnetic topologies, though the exact excitation mechanism for transverse Alfvénic oscillations remains under debate. In a very recent work by Miriyala et al. (2025), a new approach was introduced in defining the photospheric driver. Rather than using a monochromatic driver, they implemented a broadband driver with frequencies distributed across the Gaussian power spectrum peaking at a 5-minute time period, which was able to produce the peak power at 4 mHz frequency in corona.

Furthermore, phenomena such as sunspot oscillations and the variation of wave power with field inclination offer observational support for the modulation of wave propagation by the magnetic environment, reinforcing the theoretical framework of *p*-mode-driven Alfvénic wave generation through structured magneto-atmospheres Jess et al. (2013); Felipe et al. (2010). Subsequent work by Skirvin and Van Doorsselaere (2024) laid down the importance of transverse structuring on wave mode conversion. Their simulations revealed that inhomogeneities in the magnetic field and plasma structure can facilitate mode conversion processes within the chromosphere and transition region.

Nevertheless, the question of how much energy such waves can transport into the corona, and whether p-mode coupling is a dominant mechanism for coronal wave generation and heating is still open.

1.7 Objectives

The objectives of this thesis is to examine wave dynamics and transient events in the solar atmosphere through numerical simulations to study the energy transport in different layers of the atmosphere. Our specific goals are,

- 1. **Develop a comprehensive numerical MHD model** that simulates the solar atmosphere from the convection zone to the corona, capable of capturing wave propagation, mode conversion, and energy transport across stratified layers.
- 2. **Investigate the role of photospheric** p**-mode oscillations** in driving magnetohydrodynamic (MHD) wave modes (slow, fast, and Alfvén waves), and assess their efficiency in transporting energy upward through different atmospheric layers, particularly focusing on mode conversion in regions of varying plasma- β .
- 3. Study the interaction between transient events such as solar jets and global *p*-mode oscillations, to understand how such interactions influence wave dynamics, energy transfer, and coronal power spectrum.

Chapter 2

Methodology

The first chapter introduced the overview of the solar atmosphere and defined the coronal heating problem. We also discussed the steps that are needed to be taken to approach this issue. But for us the first step is to develop a numerical model of quite sun in which we can further study the plasma and thermal processes. We developed a gravitationally stratified solar atmosphere governed by MHD equations.

$$\frac{\partial \rho}{\partial t} + \nabla \cdot (\rho \vec{v}) = 0 \tag{2.1}$$

$$\frac{\partial(\rho\vec{v})}{\partial t} + \nabla \cdot \left| \rho \vec{v} \vec{v}^T + \left(p + \frac{\vec{B} \cdot \vec{B}}{2} \right) \mathbf{I} - \vec{B} \vec{B}^T \right| = \rho \vec{g}$$
 (2.2)

$$\frac{\partial \vec{B}}{\partial t} + \nabla \cdot (\vec{v}\vec{B} - \vec{B}\vec{v}) = -\nabla \times (\eta \nabla \times \vec{B})$$
(2.3)

$$\frac{\partial e}{\partial t} + \nabla \cdot \left[\left(e + p + \frac{\vec{B}^2}{2} \right) \vec{v} - (\vec{v} \cdot \vec{B}) \vec{B} \right] = Q \tag{2.4}$$

$$\nabla \cdot \vec{B} = 0 \tag{2.5}$$

Here e is total energy density which is defined as,

$$e = \frac{p}{\Gamma - 1} + \frac{1}{2}\rho|\vec{v}|^2 + \frac{\vec{B}^2}{2}$$
 (2.6)

Where,

Here, ρ represents the mass density [g cm⁻³], and \vec{v} denotes the velocity field [cm s⁻¹]. The thermal pressure is given by p [dyn cm⁻²], while \vec{B} corresponds to the magnetic field [G]. The

magnetic diffusivity is represented by η [cm² s⁻¹], and \vec{g} stands for the gravitational acceleration [cm s⁻²]. The total energy density is denoted by e [erg cm⁻³], and Q represents the energy source or sink term [erg cm⁻³ s⁻¹]. Lastly, Γ is the adiabatic index, which is set to 5/3 for an ideal gas.

In ideal plasma, we can assume an equal number of electrons and ions, so the net electric field is approximated to zero, so we only need four quantities, density ρ , mean velocity \vec{v} , pressure p and magnetic field \vec{B} . The MHD equation that governs the dynamics of the plasma are as follows:

It is important to question whether MHD approximation applies in the solar atmosphere? One important condition for the applicability of fluid dynamics in any system is that it has to be collisional. The solar atmosphere is weakly collisional, and physical collisions rarely occur in the corona. However, the mean free path of particle collision is around 3 cm in the chromosphere and 30 km in the corona. This dynamical length scale is much shorter than the length of our system, which is 10,000 km. And even if the corona is weakly collisionless, MHD is still applicable because the conservation laws of mass, momentum, and energy are still applicable and it captures the constraints imposed by gyro-motion and wave-particle interactions very well. (Priest (2019))

2.1 PLUTO code

PLUTO is a widely utilized code by astrophysicists to analyze astrophysical plasma and simulate diverse astrophysical systems, including AGNs, jets, accretion disks, interstellar gas clouds, and stellar atmospheres.

PLUTO integrates the system of conservation laws, which is generalized in form of,

$$\frac{\partial \vec{U}}{\partial t} = -\nabla \cdot \mathbf{T}(\vec{U}) + S(\vec{U}),$$

where \vec{U} denotes the state vector of conserved quantities, $\mathbf{T}(\mathbf{U})$ is a rank-2 tensor which represents the flux, and $S(\mathbf{U})$ is the source term. The conservation equations are solved for rectangular grids which are defined in orthogonal curvilinear coordinates that can either be uniform or stretched.

It employs a conservative framework utilizing finite volume or finite difference methods to resolve hydrodynamic equations with shock-capturing Godunov-type algorithms. One of the advantages of using PLUTO is it offers flexible options to customize the simulation setup to fit well with the astrophysical system. For time stepping, it offers methods like RK schemes, MUSCL-Hancock for hyperbolic PDEs, and Super-Time-Stepping or RK-Legendre for efficient handling of parabolic terms. The reconstruction schemes include slope-limited TVD, PPM, WENO, and MP5, ensuring high accuracy and reduced oscillations. For Riemann solvers,

options like Roe, HLLD, HLLC, and Two-Shock handle sharp features, while simpler solvers like HLL and Lax-Friedrichs are available for general use. This modular approach supports diverse physical problems (Mignone et al. (2007)).

In PLUTO, parallelization is accomplished through domain decomposition, wherein the global computational domain is divided into subdomains containing an equal number of points, with each subdomain allocated to a processor. Subdomains are initially configured to be as cubic as feasible. However, customization can occur during runtime to restrict subdivision in particular directions. The code utilizes the MPI library for parallelization, which ensures effective communication between processors.

The modular design of PLUTO also allows the inclusion of non-ideal effects in MHD equations such as Hall MHD, Resistivity, Thermal conduction, Viscosity, and Optically Thin Cooling. For controlling the divergence condition ($\nabla . \vec{B} = 0$), PLUTO employs three methods: (1) eight wave formulation which was introduced by Powell (1994), (2) divergence cleaning technique of Dedner et al. (2002), and (3) constrained transport method.

2.2 Numerical Setup

For our study, we simulate wave propagation in the solar atmosphere by solving the equations of magnetohydrodynamics (MHD). The model assumes a gravitationally stratified atmosphere in hydrostatic equilibrium, where we include both oblique and arcade-like magnetic field configurations. Below we outline the initial and boundary conditions used, as well as the nature of the drivers applied at the bottom boundary. To build a model in PLUTO, we'll need to define initial conditions, boundary conditions and photospheric driver.

2.2.1 Initial Condition

To model the solar atmosphere, we begin with a gravitationally stratified atmosphere in hydrostatic equilibrium. The balance of forces is governed by the hydrostatic pressure balance equation:

$$-\nabla p + \rho \mathbf{g} = 0, \tag{2.7}$$

where p is the gas pressure, ρ is the mass density, and \mathbf{g} is the gravitational acceleration. Near the solar surface, the gravitational acceleration is taken to be constant with a value $g = 2.73 \times 10^4 \text{ cm/s}^2$.

Assuming an ideal gas, the equilibrium pressure and density profiles varying along the vertical y-direction are given by:

$$p(y) = p_0 \exp\left(-\int_{y_0}^{y} \frac{\hat{m}gdy'}{k_B T(y')}\right), \qquad (2.8)$$

$$\rho(y) = \frac{p(y)\hat{m}}{k_B T(y)},\tag{2.9}$$

where T(y) is the temperature profile taken from the VAL-C model Vernazza et al. (1981), \hat{m} is the mean particle mass, k_B is the Boltzmann constant, p_0 is the pressure at the reference height y_0 , and y is the vertical coordinate.

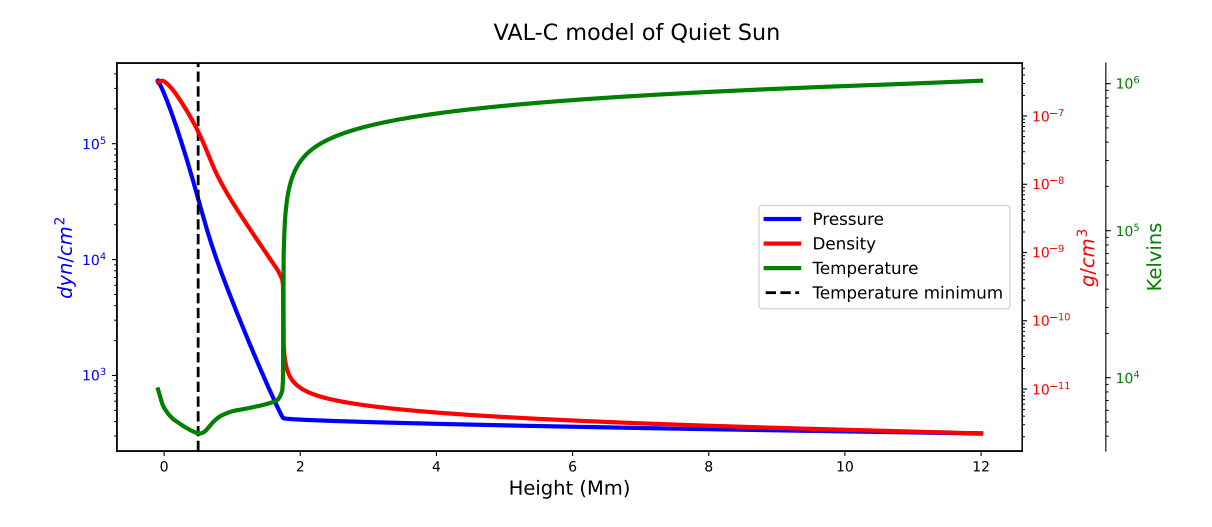


Figure 2.1: Initial profile of hydrostatic solar atmosphere

Our model extends from -90km to 12,000km with stretched grids with 100 grids between the height of -90km to 1500km, 200 grids between 1,500km to 2,500km, and 300 grids between 2,500km to 12,000km. This grid spacing is important to resolve the transition region as the density height scale at transition regions is 3-5km. which is given by,

$$H = -\left(\frac{1}{\rho}\frac{d\rho}{dy}\right)^{-1} \tag{2.10}$$

In the x-axis, our domain spans from -4,000km to 4,000km with a uniform grid spacing of 500 grids.

In numerical simulations of wave propagation in sunspot-like regions, it is crucial to initialize the model in a state of equilibrium that reflects the physical conditions of the solar atmosphere. Sunspots are regions of strong magnetic field concentrations (> 1 KG) where the magnetic pressure plays a significant role in the force balance. As a result, many sunspot models (like Khomenko et al. (2008)) adopt a magnetostatic model in which the sum of gas pressure, magnetic pressure, and magnetic tension forces are balanced.

However, in our setup, we initialize the atmosphere in hydrostatic equilibrium, meaning that only the balance between the vertical pressure gradient and gravity is considered at the

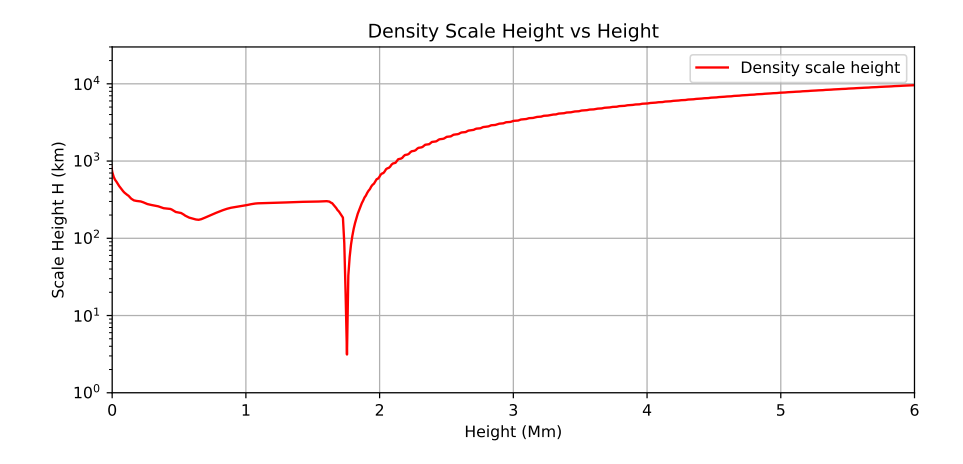


Figure 2.2: Plot for density height scale

initial state. For magnetic field we ensure a force-free field such that;

$$\vec{J} \times \vec{B} = 0$$
 and $\nabla \times \vec{B} = 0$, (2.11)

where \vec{J} is the current density and \vec{B} is the magnetic field. We consider two types of magnetic field configurations:

Vertical Magnetic Field: A constant, uniform magnetic field directed along the y-axis:

$$\vec{B} = 168 \,\hat{j} \quad \text{Gauss.} \tag{2.12}$$

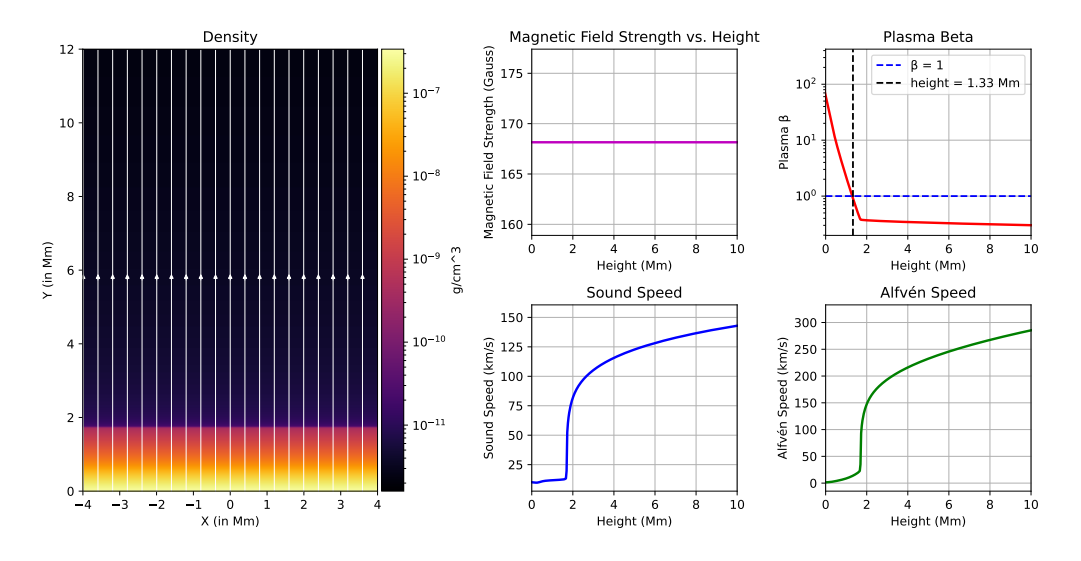


Figure 2.3: Initial profile for stratified atmosphere with oblique magnetic field

Arcade Magnetic Field: This is modeled using a magnetic vector potential $\vec{A} = A(x,y)\hat{z}$, following the formulation of Low (1985) which describes a force-free field for solar arcade-like structures:

$$\vec{B} = \nabla \times A\hat{z},\tag{2.13}$$

$$A(x,y) = \frac{x(y_{\text{ref}} - b)^2}{(y - b)^2 - x^2} B_{\text{ref}},$$
(2.14)

where b is the depth of the magnetic source, $y_{ref} = 10$ Mm is the reference height, and B_{ref} is the magnetic field strength at this height.

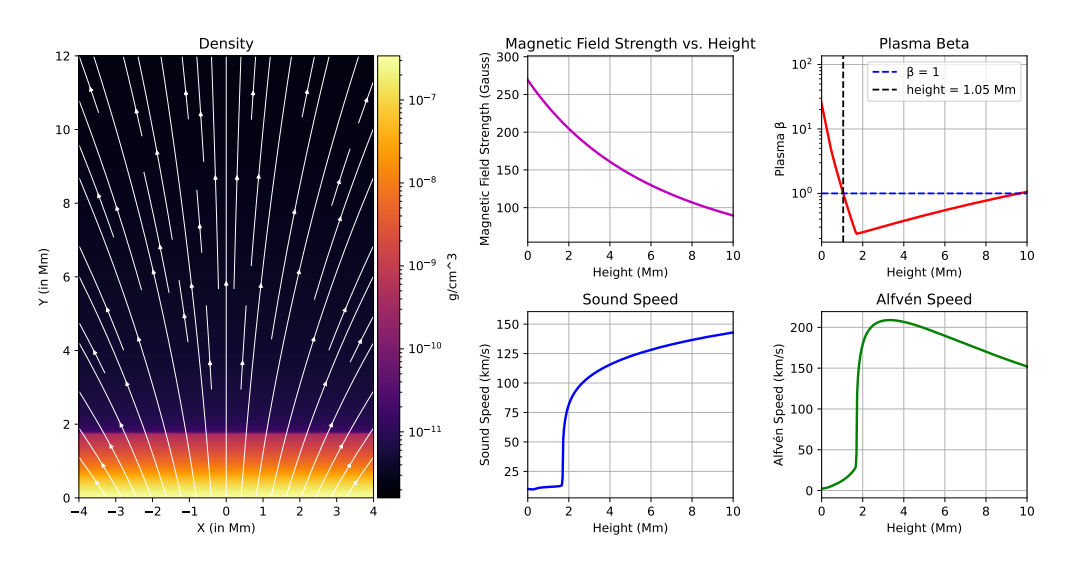


Figure 2.4: Initial profile for stratified atmosphere with arcade magnetic field

2.2.2 Boundary Conditions

Boundary conditions play a crucial role in the accuracy and stability of numerical simulations, especially when modeling complex systems like the solar atmosphere. In our setup, the boundaries are designed to minimize unphysical reflections and ensure the consistency of the physical properties across the entire computational domain. Properly chosen boundary conditions not only preserve the realism of the simulated system but also allow for the seamless propagation of wave structures and the accurate representation of dynamic behaviors at the boundaries.

Top Boundary (Sponge Layer) To prevent unphysical reflections of outgoing waves from the upper boundary, we implement a sponge (absorbing) layer at the top of the simulation domain. This sponge layer extends from z_{db} (damping bottom) to z_{tb} (damping top), and its purpose is to smoothly attenuate the time-dependent variables as they approach the top boundary. The damping within this layer follows an exponential function:

$$u' = u \exp\left(-a \cdot \frac{z - z_{\text{db}}}{z_{\text{tb}} - z_{\text{db}}}\right),\tag{2.15}$$

where u is the original value of a time-dependent variable (e.g., velocity components), u' is the damped value, and a is a dimensionless damping coefficient that controls the strength of attenuation. This technique ensures that outgoing waves are smoothly absorbed near the

boundary, preventing any reflections that could contaminate the results. This approach is widely used in astrophysical simulations to handle the upper boundary without introducing artificial reflections such as Popescu Braileanu and Keppens (2021).

Bottom Boundary (Symmetric Boundary) At the bottom boundary of the domain, we apply symmetric boundary conditions for time-dependent variables. The symmetric boundary conditions are defined such that:

$$v_1^* = v_1$$
 and $v_2^* = v_2$, (2.16)

where v_1 and v_2 are the values of a variable in the first and second domain cells, respectively, and v_1^* and v_2^* are the corresponding values in the ghost cells adjacent to the boundary. The first ghost cell is closest to the boundary, while the second ghost cell is one step further into the domain. This symmetric behavior ensures that there is no abrupt change in the physical quantities at the boundary, allowing for smooth propagation of wave modes across the bottom of the domain.

The symmetric boundary conditions are applied to all relevant time-dependent variables, such as velocity components and the magnetic field. These conditions are essential for maintaining the stability of the simulation and ensuring that no unphysical behavior is introduced at the bottom boundary, which could distort the simulation of solar atmospheric dynamics.

Perturbations at the Bottom Boundary At the bottom boundary, only the verticle velocity components are perturbed, while other perturbative variables, such as pressure perturbation (p_1) , density perturbation (p_1) , magnetic field perturbation (B_1) , and vertical velocity (v_z) , are fixed to zero. This setup helps in isolating the perturbations to the vertical motion of the plasma, which is typical for solar atmospheric simulations that aim to study specific phenomena like convection or wave excitation at the lower boundary.

2.2.3 Photospheric Driver

To excite waves in the atmosphere, we implement a combination of two drivers, one acting on v_y and another acting on v_z . Although the simulation domain is two-dimensional in space (x-y plane), we introduce velocity perturbations in both the v_y and v_z components to model a more realistic excitation of MHD waves in the solar atmosphere. This 2.5D approach allows for the inclusion of out-of-plane dynamics—particularly Alfvénic motions. In our model, wave excitation is achieved by applying two types of drivers,

Monochromatic Driver: This driver introduces a single-frequency perturbation in the horizontal velocity component V_y with a Gaussian spatial envelope along the x-axis. The perturbation follows the formulation of Khomenko et al. (2008):

$$V_{y}(x,t) = V_{0}\sin(\omega t)\exp\left[-\frac{(x-x_{0})^{2}}{2\sigma^{2}}\right],$$
(2.17)

where V_0 is the velocity amplitude, x_0 is the center of the Gaussian envelope, σ defines the spatial width, and $\omega = 2\pi/T$ is the angular frequency, with T = 5 minutes. Velocity amplitude for our model is 400 ms^{-1} for v_v component and 200 ms^{-1} for v_z component.

Broad-band Driver: This driver introduces a spectrum of frequencies to mimic the complex, turbulent conditions of the solar photosphere. It enables the simultaneous excitation of multiple wave modes, allowing for studies of nonlinear interactions and spectral energy transfer in a more realistic setting. To mimic the power spectrum of observed p-mode oscillations, we used a Gaussian probability distribution to sample the frequencies and formulate our driver. We not only have random frequencies in our driver, but also different magnitudes to mimic a realistic driver (see Fig.2.6).

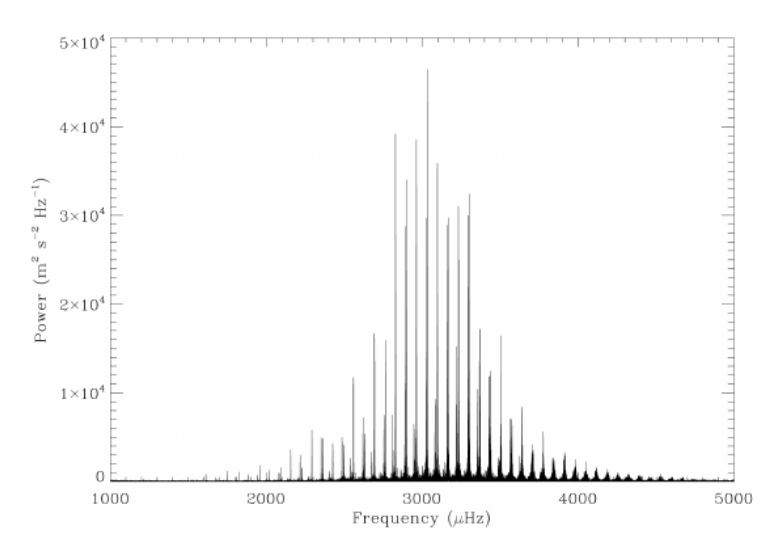


Figure 2.5: BiSON spectrum of p-mode oscillation, Elsworth et al. (2015).

2.3 Launching Solar Jet

To investigate the dynamics of solar jets and their interaction with the global p-mode oscillation, we initiate a localized pressure perturbation at chromospheric heights within the simulation domain. This technique emulates the impulsive energy release events in the solar chromosphere, such as those triggered by small-scale magnetic reconnection, shock waves, or convective buffeting, which are believed to drive jet-like plasma motions in the lower solar atmosphere.

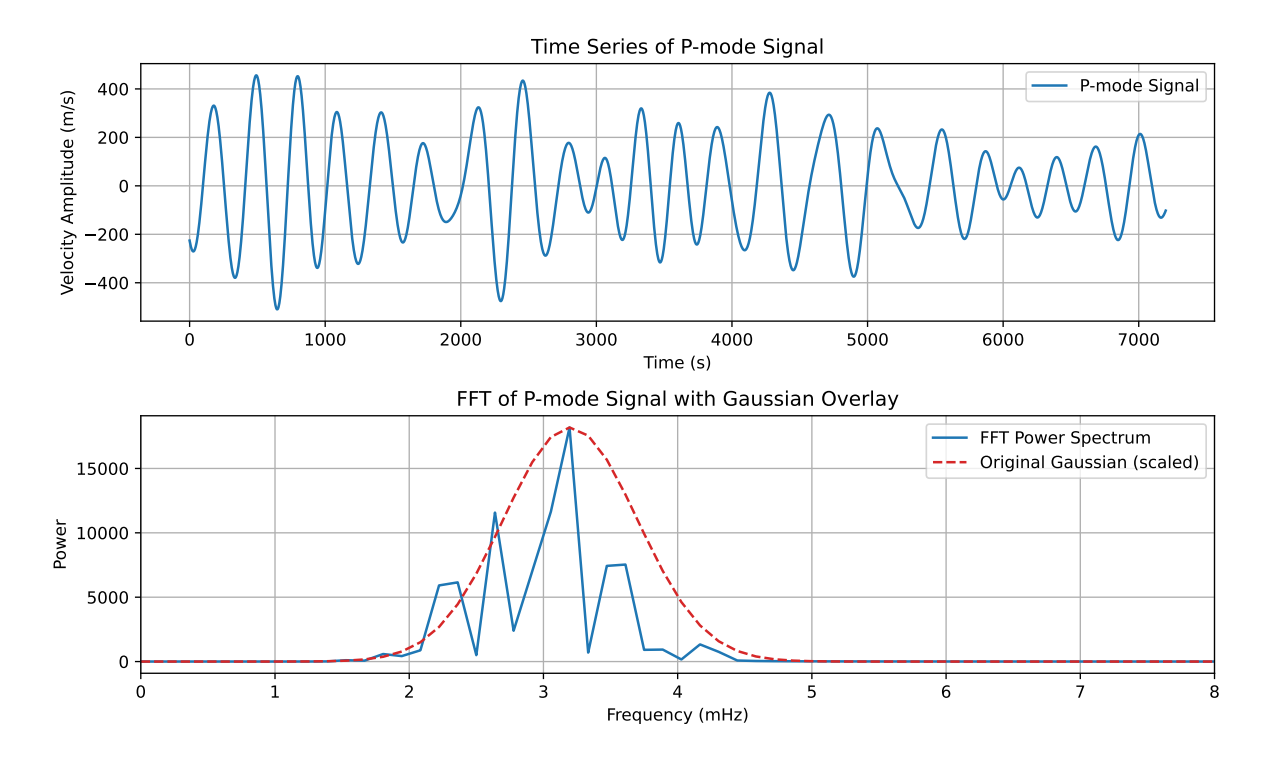


Figure 2.6: Broad-band power spectrum and velocity timeseries

The pressure perturbation is applied in the form of a Gaussian pulse superimposed on the background plasma pressure at a specific location and time. The perturbation is spatially confined and temporally impulsive to mimic a localized, transient energy deposition event. The form of the perturbation is given by:

$$p_1(x, y, t) = A_p \exp\left[-\frac{(x - x_0)^2}{w_x^2} - \frac{(y - y_0)^2}{w_y^2}\right]$$
 (2.18)

where A_p is the perturbation amplitude, (x_0, y_0) marks the perturbation center and w_x and w_y control the spatial extent of the perturbation in the x and y directions. This perturbation produces an upward-propagating pressure pulse that launches a jet of chromospheric plasma into the overlying atmosphere. This way launching impulsive pressure-driven jet has been studied extensively by Singh et al. (2019) and offers common resemblance for the evolution of different solar jets which have been observed to have heating at the base.

The plasma response to the combined effect of the localized jet-driving perturbation and the ambient *p*-mode oscillations is by studying its wave response. To quantify the behavior of the jet and wave field, we track the following diagnostics: the vertical velocity distribution to assess the plasma uplift and decompose the MHD wave modes using the velocity projections as discussed in section 2.4, revealing the role of fast, slow, and Alfvénic components in the jet evolution.

This setup provides a controlled environment to study how localized plasma ejections interact with the ubiquitous wave motions in the solar atmosphere and whether such interactions

can enhance energy transport and contribute to chromospheric and coronal heating.

2.4 Analysis

To understand the nature and impact of the wave dynamics in the solar atmosphere, a thorough analysis of the simulation data has been performed. This section delves into the key diagnostics that help interpret how waves behave, interact with the background plasma, and contribute to energy transport. The focus is on quantifying mode conversion, the spectral distribution of wave power, and energy transport in various forms—crucial for identifying possible mechanisms of chromospheric and coronal heating.

The initial part of the analysis focuses on investigating wave mode conversion and the temporal evolution of various wave modes as they propagate through different layers of the solar atmosphere. By decomposing the velocity and magnetic field perturbations into longitudinal, transverse, and Alfvénic components, it becomes possible to distinguish the nature of the wave modes — whether fast, slow, or Alfvén — and monitor their mutual conversion over time. This approach is fundamental to understanding how the geometry of the magnetic field and the plasma β parameter govern the propagation and transformation of MHD waves. In particular, when the background magnetic field lies within the x-y plane, the velocity perturbations can be decomposed by projecting the velocity vector \mathbf{u} as:

$$v_{\text{Alfvén}} = \mathbf{u} \cdot \hat{z},\tag{2.19}$$

$$v_{\text{slow}} = \mathbf{u} \cdot \hat{\mathbf{s}},\tag{2.20}$$

$$v_{\text{fast}} = \mathbf{u} \cdot (\hat{z} \times \hat{s}), \tag{2.21}$$

where \hat{s} is the unit vector along the in-plane magnetic field direction and \hat{z} is the direction perpendicular to the x-y plane. Here, $v_{\text{Alfv\'en}}$ captures the out-of-plane Alfv\'enic motion, v_{slow} represents compressive motion along the magnetic field, and v_{fast} captures transverse magnetoacoustic motions. This decomposition enables us to quantify the relative strength and evolution of each wave mode with time and height Yadav et al. (2022).

The next diagnostic involves a spectral analysis of wave power at various heights through Fourier transforms. By applying Fourier analysis to the temporal evolution of velocity components at specific heights, we extract the frequency content of wave motions. This technique helps us monitor whether specific frequencies dominate as waves propagate, and whether phenomena such as wave steepening, harmonic generation, or frequency doubling take place, shedding light on the non-linear behavior of waves.

To understand how much energy is transported by different wave modes, we compute the energy flux carried by the slow magnetoacoustic, Alfvén, and fast magnetoacoustic waves sep-

arately. Such decomposition is crucial to assess the relative importance of each wave mode in energy transport and their contribution to atmospheric heating. The expressions used for calculating the energy fluxes, as adopted from Yadav et al. (2022), are:

$$F_{\text{slow}} = \rho \, v_{\text{slow}}^2 \, c_s, \tag{2.22}$$

$$F_{\text{Alfv\'en}} = \rho \, v_{\text{Alfv\'en}}^2 \, v_A, \tag{2.23}$$

$$F_{\text{fast}} = \rho \, v_{\text{fast}}^2 \, \sqrt{c_s^2 + v_A^2},$$
 (2.24)

where ρ is the plasma density, v_{slow} , $v_{\text{Alfvén}}$, and v_{fast} are the decomposed velocity components, c_s is the local sound speed, and v_A is the Alfvén speed. These expressions combine the ram pressure of each wave mode with its group velocity, giving a consistent estimate of the energy carried. Importantly, even in the case of standing waves—where the net acoustic or magnetic energy flux might be zero due to phase cancellations—the individual energy fluxes remain positive and meaningful Felipe et al. (2010). This approach thus provides a clearer picture of energy transfer during wave-mode interactions.

In addition to mode-separated fluxes, we compute the total wave energy flux using both acoustic and electromagnetic components. This provides a more global measure of energy transfer that does not rely on prior wave decomposition. The expression used is:

$$F_{wave} = p_1 v + B_1 \times (u \times B_0), \tag{2.25}$$

where the first term represents the acoustic wave flux and the second term is the Poynting flux.

Finally, we examine the spatial and temporal distribution of energy densities—specifically the kinetic and magnetic components. Monitoring how these forms of energy evolve over time helps us identify areas where wave energy is being stored, dissipated, or converted into heat. This diagnostic is vital in revealing regions of wave damping and assessing the efficiency of various heating mechanisms operating across the solar atmosphere.

Chapter 3

Results and Discussions

We devised the following experiments with a model to study the wave propagation and evolution with time in different magnetic fields perturbed with different photospheric drivers, as we discussed in Chapter-2. Here, we present the results of the experiments and provide a detailed discussion of the findings.

3.1 Monochromatic driver

As we discussed in Chapter-2, a monochromatic driver uses a sine wave to perturb the velocity components in the y and z axes to generate longitudinal and transverse waves. We'll see its effect in two different magnetic field configurations and establish the role of transverse structuring of the magnetic field in energy propagation.

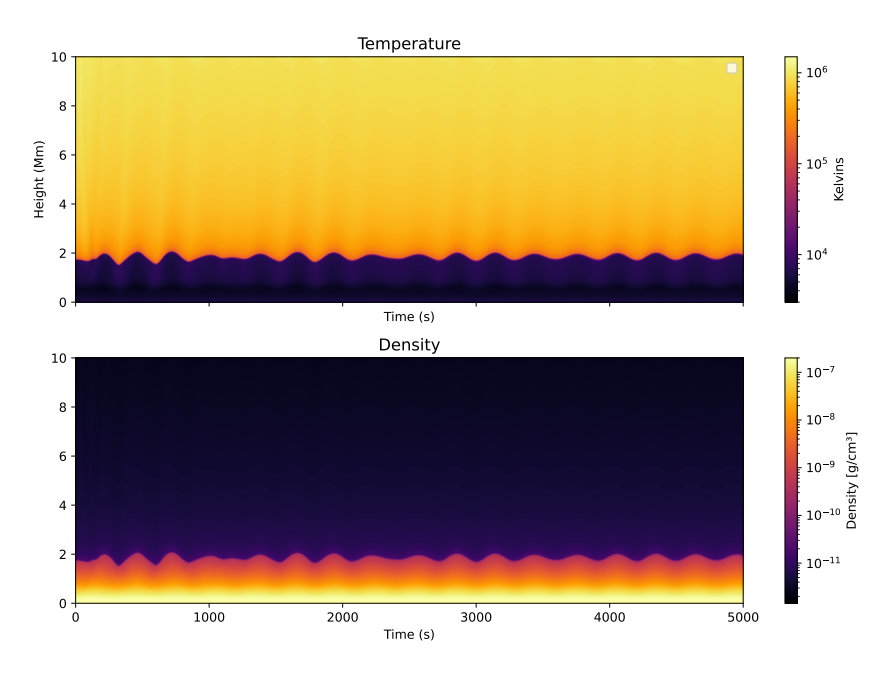


Figure 3.1: Temporal evolution of temperature and density profiles under the influence of a monochromatic driver in an arcade magnetic field configuration.

3.1.1 Vertical magnetic field

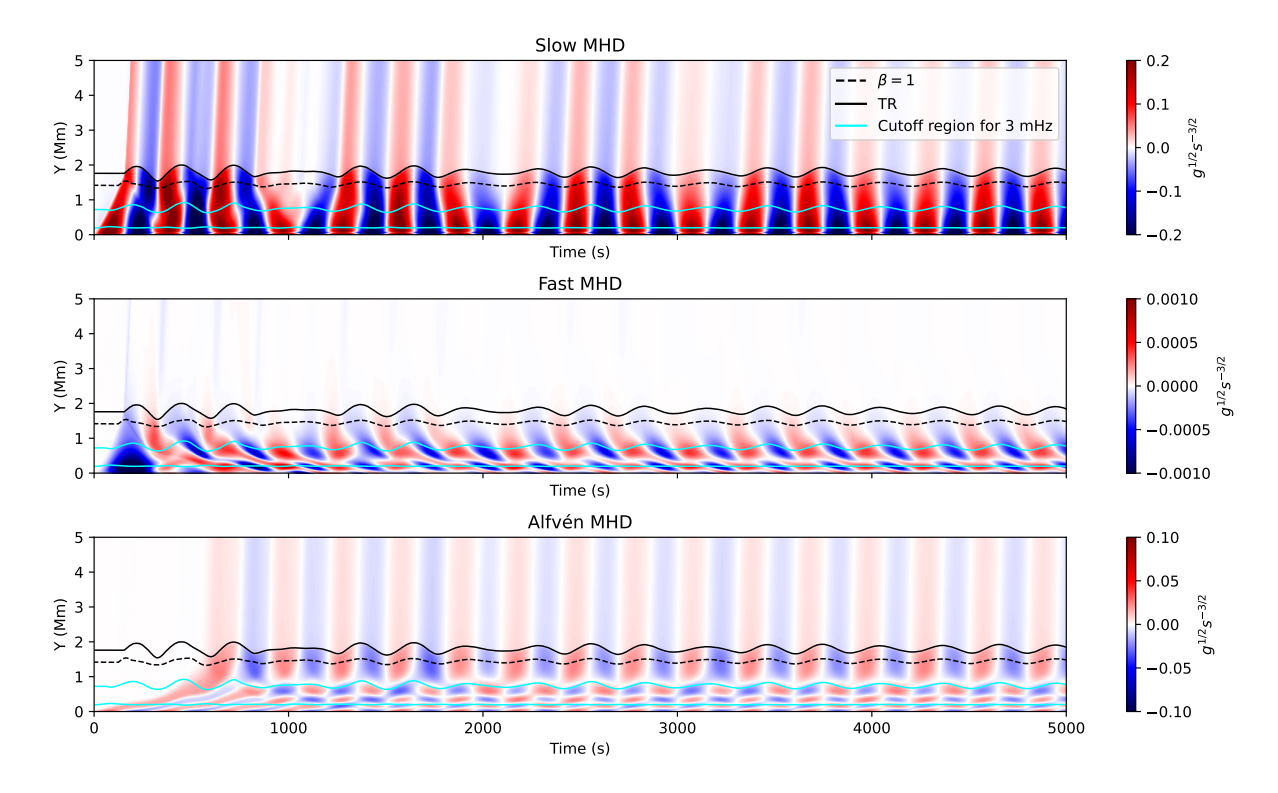


Figure 3.2: Temporal evolution of MHD variables at the center of the domain for a vertical magnetic field subjected to a monochromatic driver.

Figure 3.2 shows the time evolution of the velocity components associated with all three MHD wave modes, scaled by a factor of $\sqrt{\rho v_{ph}}$, where $v_{ph} = c_s$ for the slow mode, $v_{ph} = \sqrt{c_s^2 + v_A^2}$ for the fast mode, and $v_{ph} = v_A$ for the Alfvén mode. This scaling serves as a proxy for the temporal evolution of the wave energy fluxes, following the approach of Khomenko et al. (2008).

The slow mode is observed to reach the transition region, with a fraction of its energy transmitted into the corona, consistent with the findings of Santamaria et al. (2015). However, a significant portion of the slow mode is reflected at the transition region, where the sharp gradients in density and pressure act as a partial mirror Roberts (2006). This reflection establishes a resonance cavity — a region where waves are trapped between reflective boundaries, forming standing wave patterns. Another source of reflection is the sponge layer, which, although designed to absorb vertically propagating perturbations, is less effective for those traveling horizontally. Consequently, while reflections in the longitudinal component are minimal, residual reflections persist in the transverse components.

Mode conversion from slow to fast modes is also apparent near the $\beta = 1$ layer. The fast mode emerges due to the spatial dependence of the v_y perturbation, which induces additional motion along the x-axis. These fast waves, however, are reflected at the transition region and do not transmit energy into the corona, indicating that magnetic energy cannot escape through

the fast MHD mode.

The Alfvén mode initially propagates upward at a relatively slow rate due to the low Alfvén speed in the lower atmosphere, as shown in Figure 2.3. Above the transition region, however, the Alfvén speed increases significantly, and the Alfvén wave velocity surpasses the sound speed of the slow mode. Similar to the other modes, Alfvén waves experience partial reflection at the transition region. A standing wave pattern forms in the lower chromosphere due to interference between upward-propagating and reflected waves. Nevertheless, a portion of the Alfvén wave energy successfully transmits through the transition region into the corona.

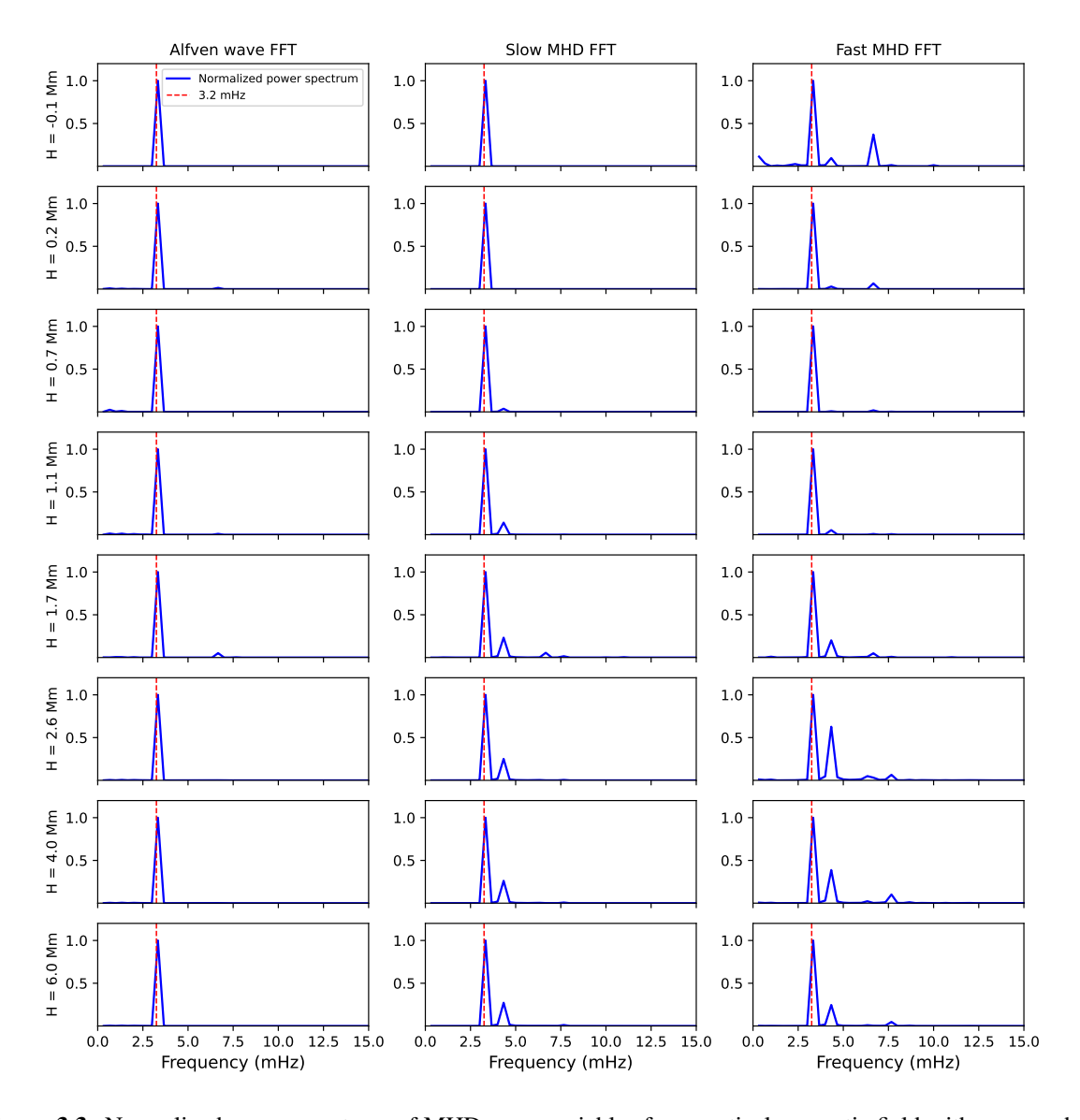


Figure 3.3: Normalized power spectrum of MHD wave variables for a vertical magnetic field with a monochromatic driver, showing a dominant peak at 3.2 mHz.

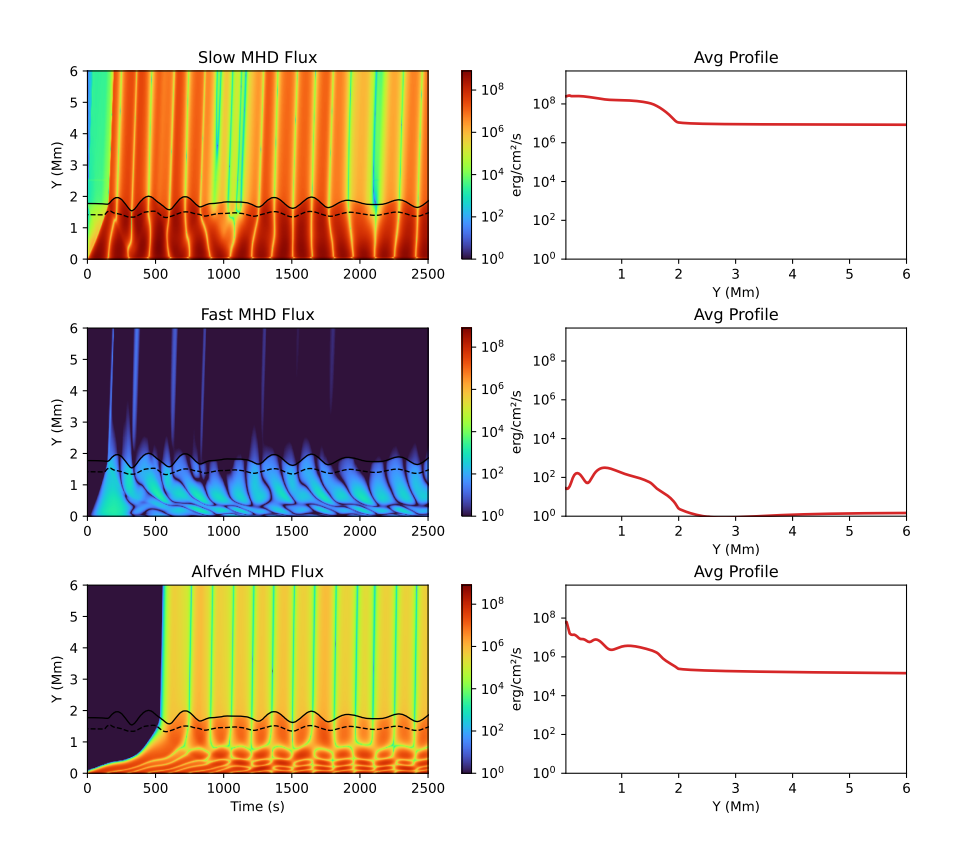


Figure 3.4: Energy flux components associated with slow, fast, and Alfvén modes in a vertical magnetic field driven by a monochromatic driver.

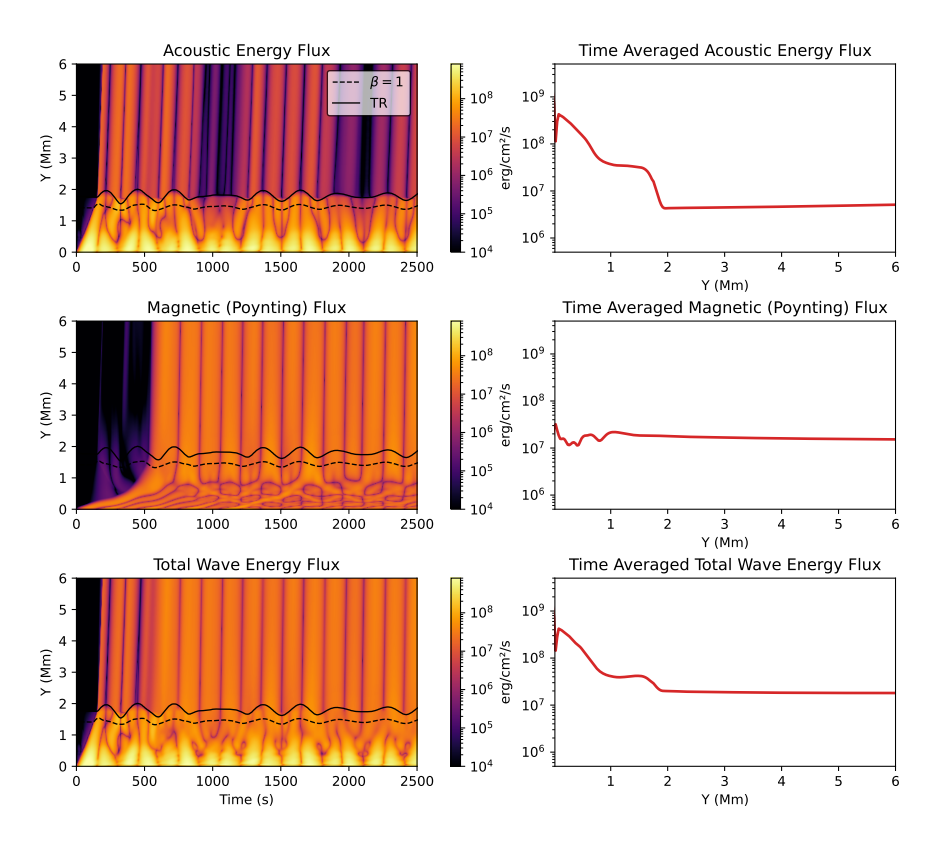


Figure 3.5: Acoustic, magnetic and total energy flux as a function of height for a vertical magnetic field with a monochromatic driver.

Figure 3.3 presents the normalized power spectra for all three wave modes. Each spectrum displays a dominant peak at 3.2 mHz, corresponding to the frequency of the imposed driver. A modest enhancement is also evident at frequencies above 4, mHz, particularly in the region above the transition region, although the associated power remains substantially lower than that at the driver frequency.

Figures 3.4 and 3.5 illustrate the energy flux transported by the three wave modes, delineating the contributions from both acoustic and magnetic components. The results indicate that acoustic energy is predominantly confined within the chromosphere, while magnetic energy — primarily conveyed by Alfvén waves — is transmitted efficiently into the corona. This behavior underscores the pivotal role of Alfvén waves in facilitating upward energy transport through the solar atmosphere.

3.1.2 Arcade magnetic field

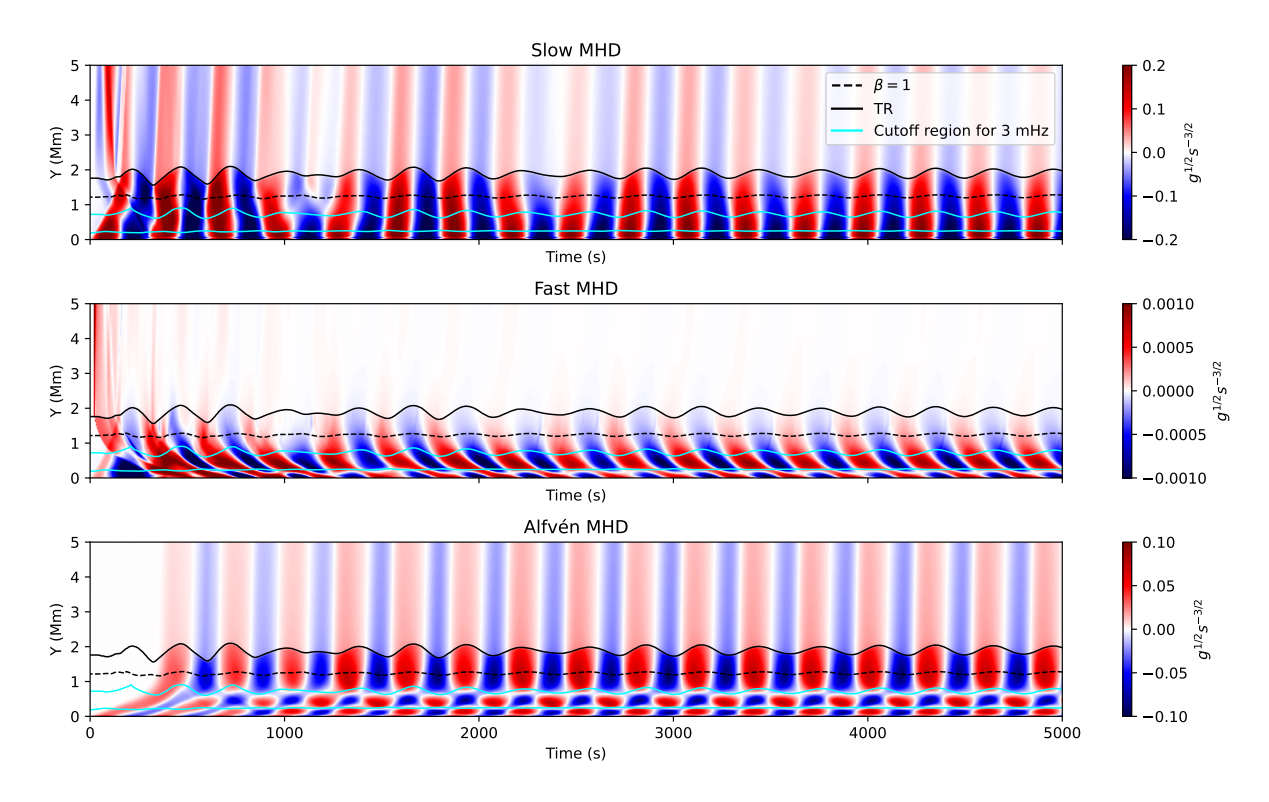


Figure 3.6: Temporal evolution of MHD wave variables at the center of the domain for an arcade magnetic field driven by a monochromatic source.

In Figure 3.15, the time series evolution of MHD wave modes in an arcade magnetic field configuration is presented. During the initial stages of the simulation, transient perturbations are observed as the system adjusts to achieve equilibrium between the magnetic field and the initial hydrostatic conditions. Owing to the stronger magnetic fields at the footpoints, both fast and Alfvén modes exhibit enhanced amplitudes in these regions.

Figure 3.23(b) illustrates that Alfvén waves, in particular, are responsible for transporting a larger fraction of the energy along the magnetic field lines. This behavior arises due to the transverse structuring inherent to the arcade field configuration, which facilitates efficient energy transfer via Alfvénic perturbations. These results underscore the crucial role of Alfvén waves in mediating energy transport from the photosphere into the corona.

The corresponding power spectrum reveals a dominant peak at 3.2 mHz, accompanied by a slight enhancement near 4 mHz, consistent with the behavior observed in simulations employing a purely vertical magnetic field configuration. This further reinforces the robustness of these wave-driven energy transport processes across varying magnetic topologies.

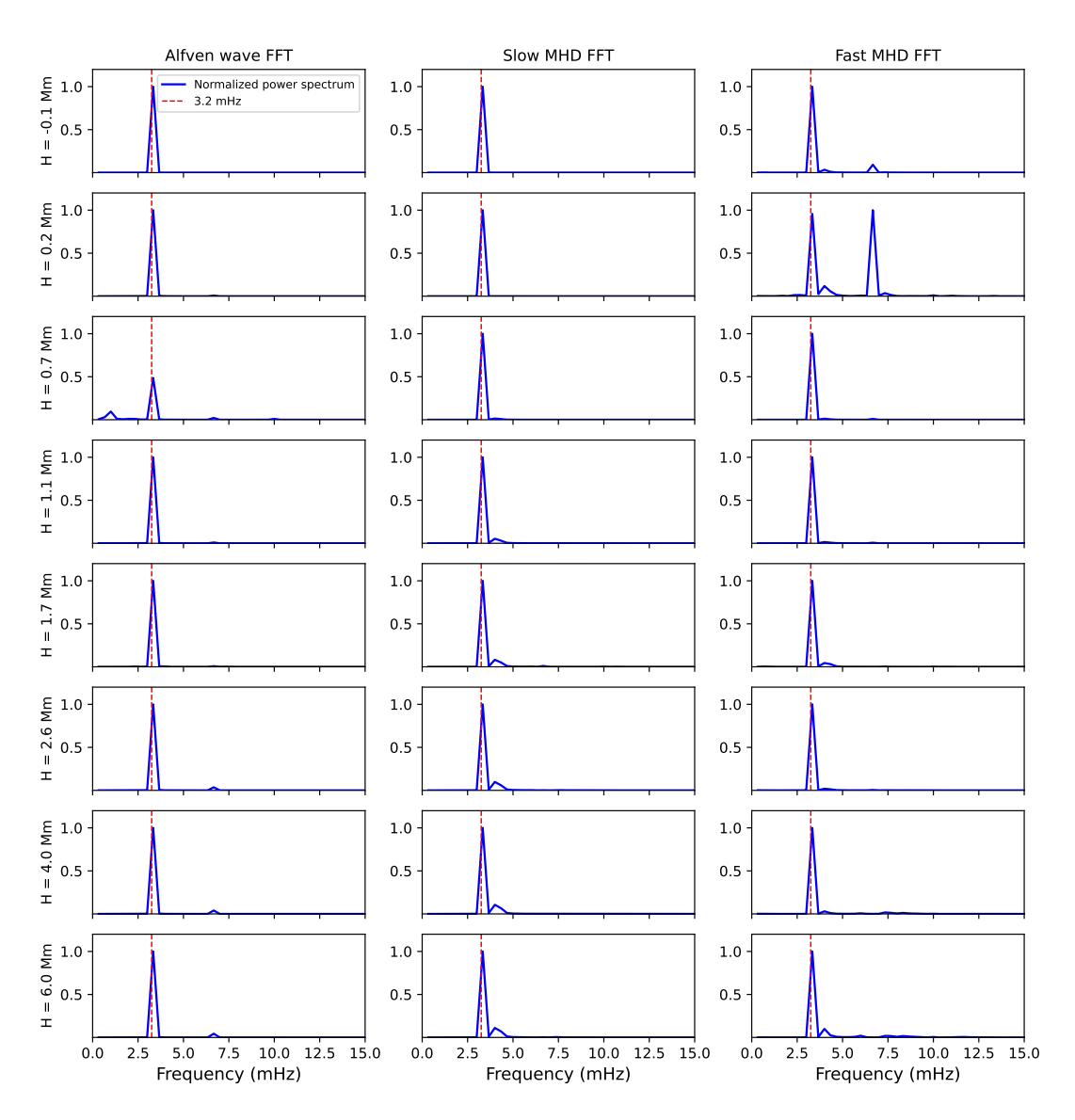


Figure 3.7: Normalized power spectrum of MHD wave variables for an arcade magnetic field with a monochromatic driver, highlighting a peak at 3.2 mHz.

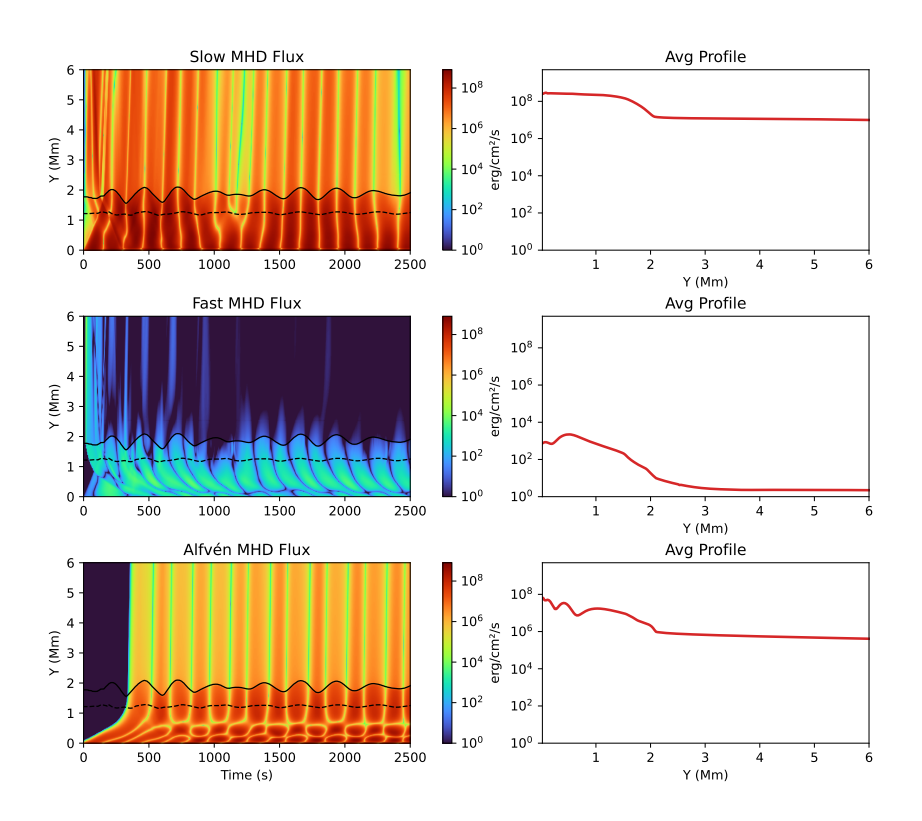


Figure 3.8: Energy flux components associated with slow, fast, and Alfvén modes in an arcade magnetic field driven by a monochromatic driver.

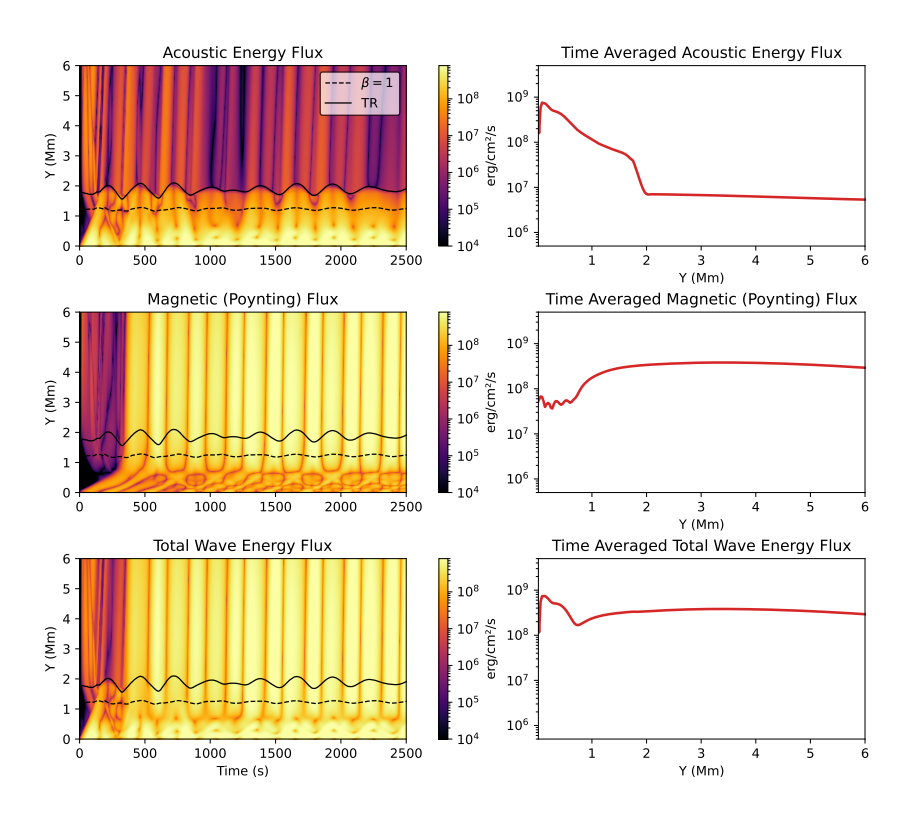


Figure 3.9: Acoustic, magnetic and total energy flux as a function of height for an arcade magnetic field with a monochromatic driver.

3.2 Broadband driver

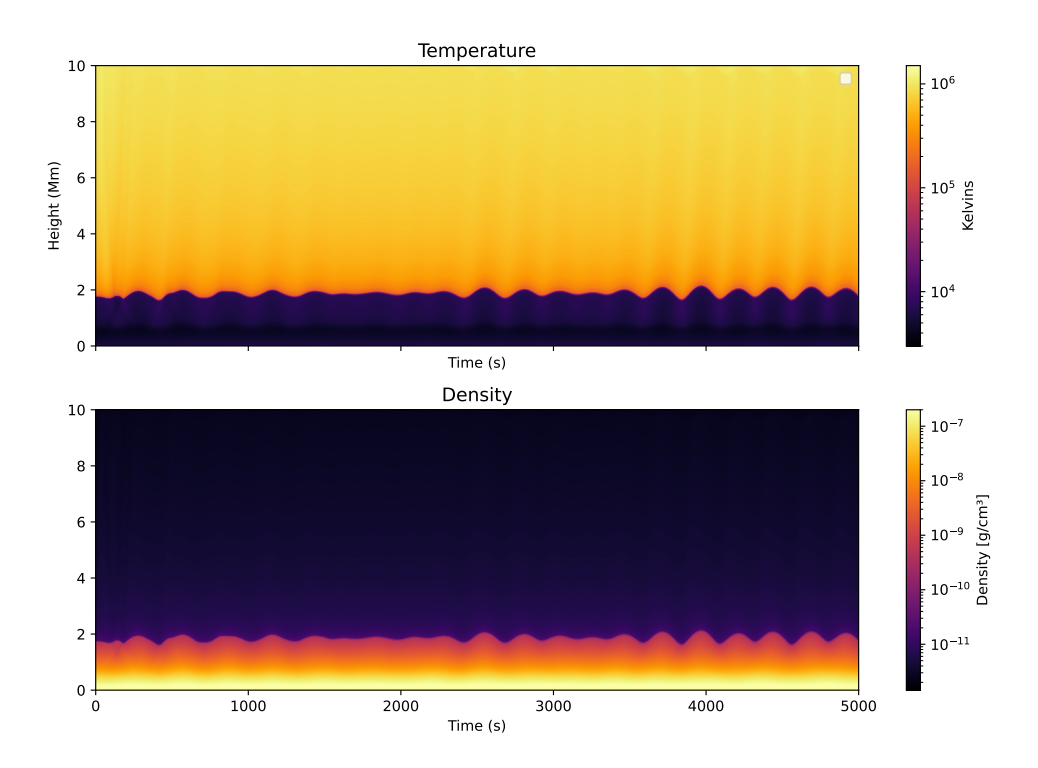


Figure 3.10: Time evolution of MHD variables at the center for vertical magnetic field with a broadband driver.

3.2.1 Vertical magnetic field

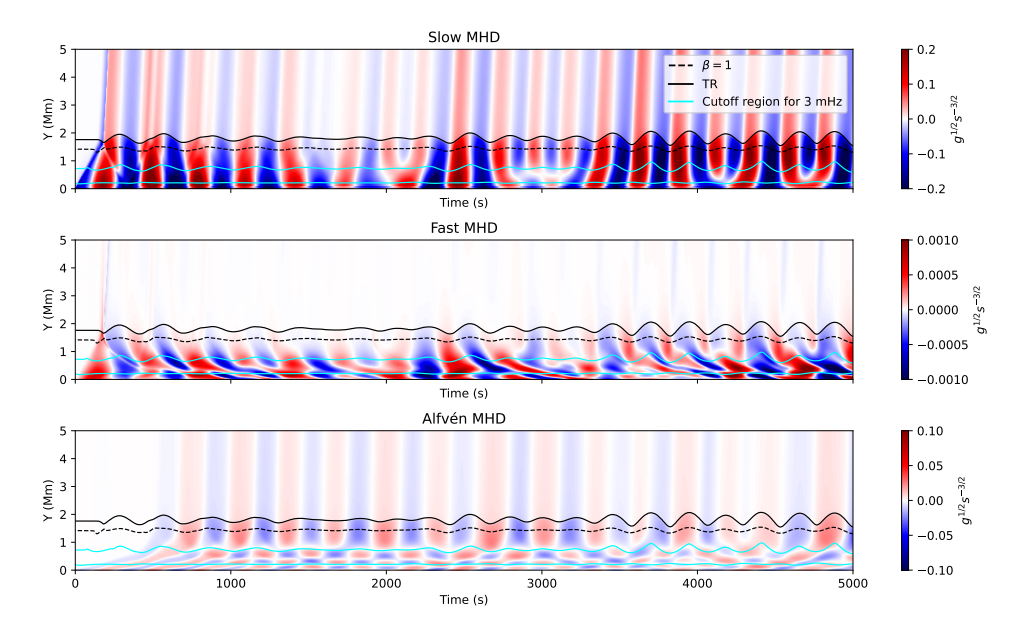


Figure 3.11: Temporal evolution of MHD wave variables at the center of the domain for a vertical magnetic field driven by a broadband source.

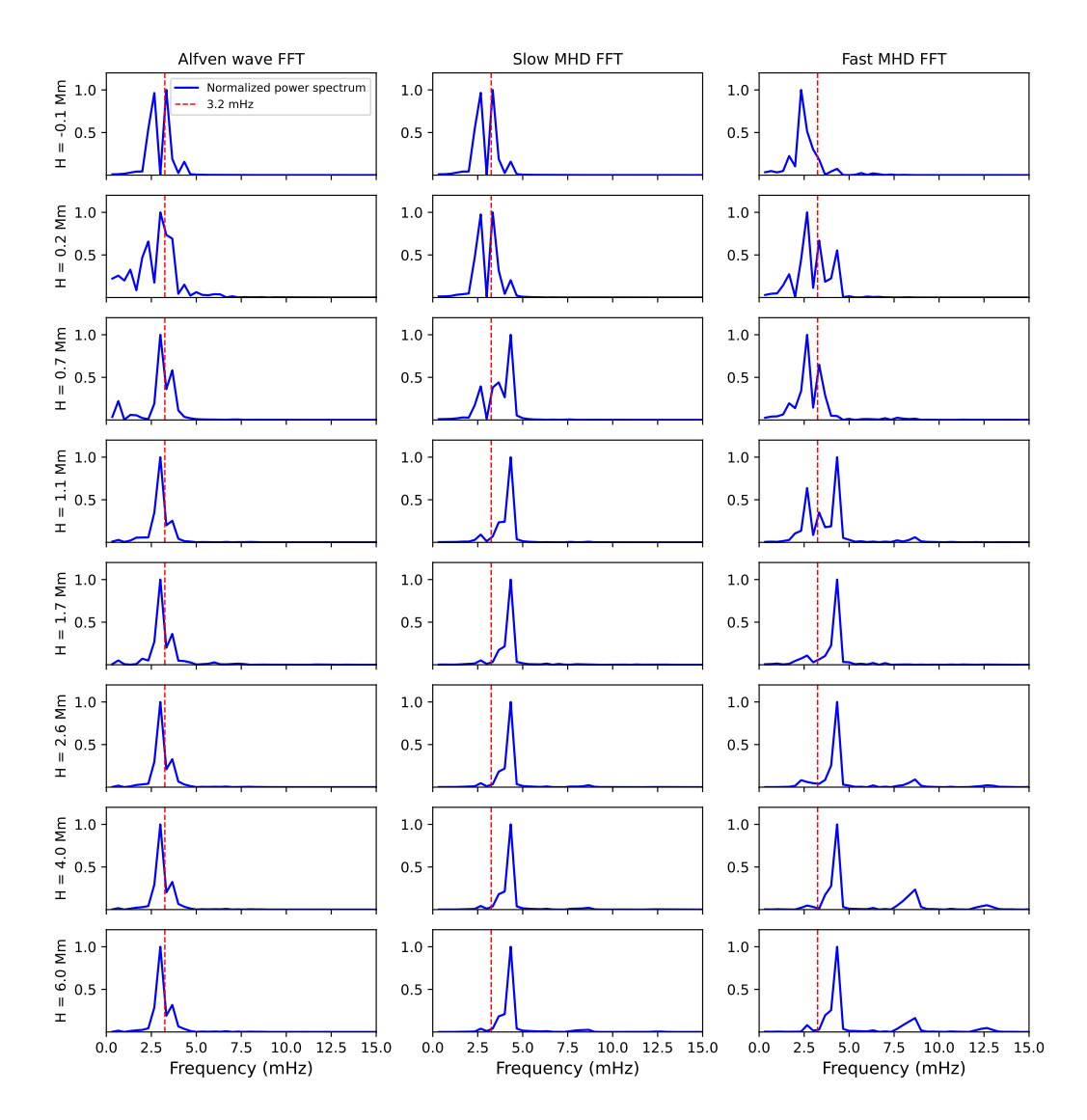


Figure 3.12: Normalized power spectrum of MHD wave variables for a vertical magnetic field with a broadband driver, showing a shift in peak power towards 4 mHz.

Wave and energy flux diagnostics show trends largely consistent with the monochromatic driver case. Notably, the power spectra of the three MHD modes reveal an overall power enhancement and a shift in the peak frequency from 3.2 mHz to around 4 mHz. While a modest increase appears in the Alfvén mode power for vertical fields, it becomes clearer and more structured in the arcade configuration (see Figure 3.16). The presence of a frequency cutoff causes the 3 mHz component to become evanescent, redistributing energy toward higher frequencies, predominantly near 4 mHz.

The additional high-frequency peak in the fast MHD spectrum arises from reflections at the sponge layer and is not considered physically significant. These results align well with the observational findings of Tomczyk et al. (2008) and Morton et al. (2015), as well as the numerical simulations by Miriyala et al. (2025), which focused on sunspot regions. Our analysis extends these insights, revealing similar spectral behavior in both vertical and arcade magnetic field

configurations within a more general solar atmosphere.

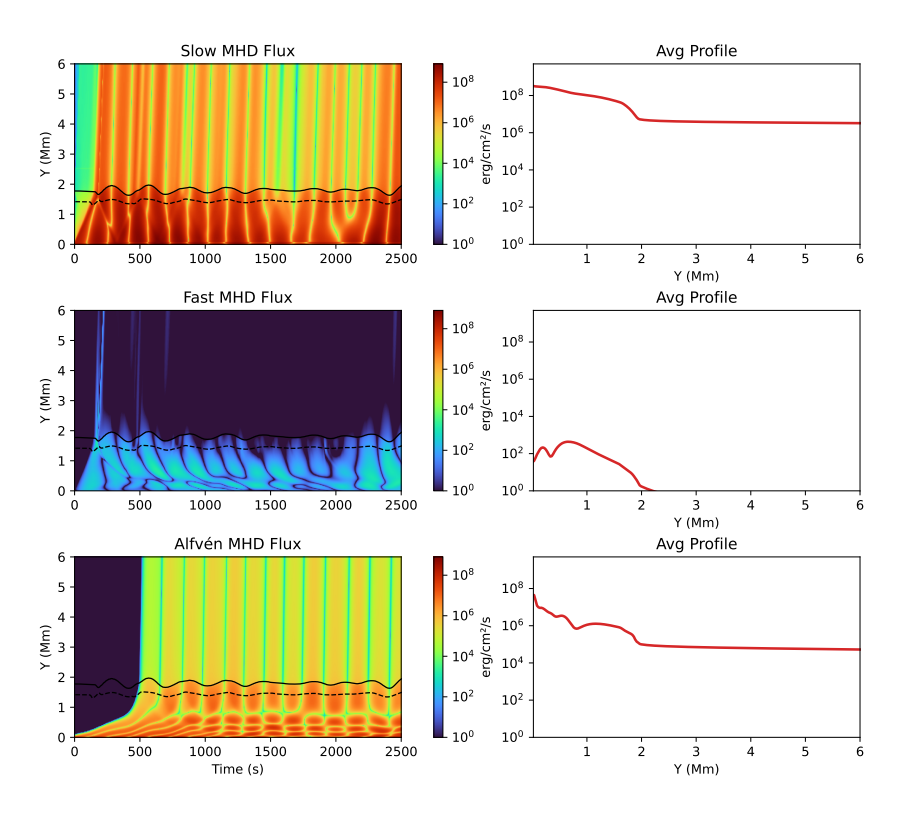


Figure 3.13: Energy flux components for slow, fast, and Alfvén modes in a vertical magnetic field driven by a broadband driver.

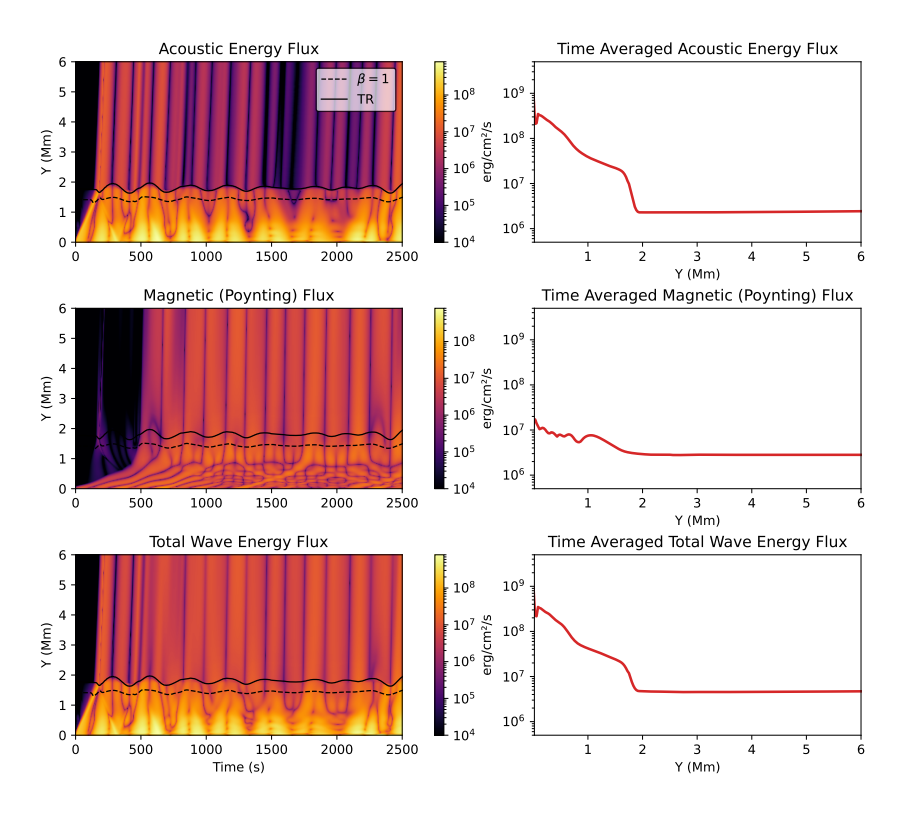


Figure 3.14: Acoustic, magnetic and total energy flux as a function of height for a vertical magnetic field with a broadband driver.

3.2.2 Arcade magnetic field

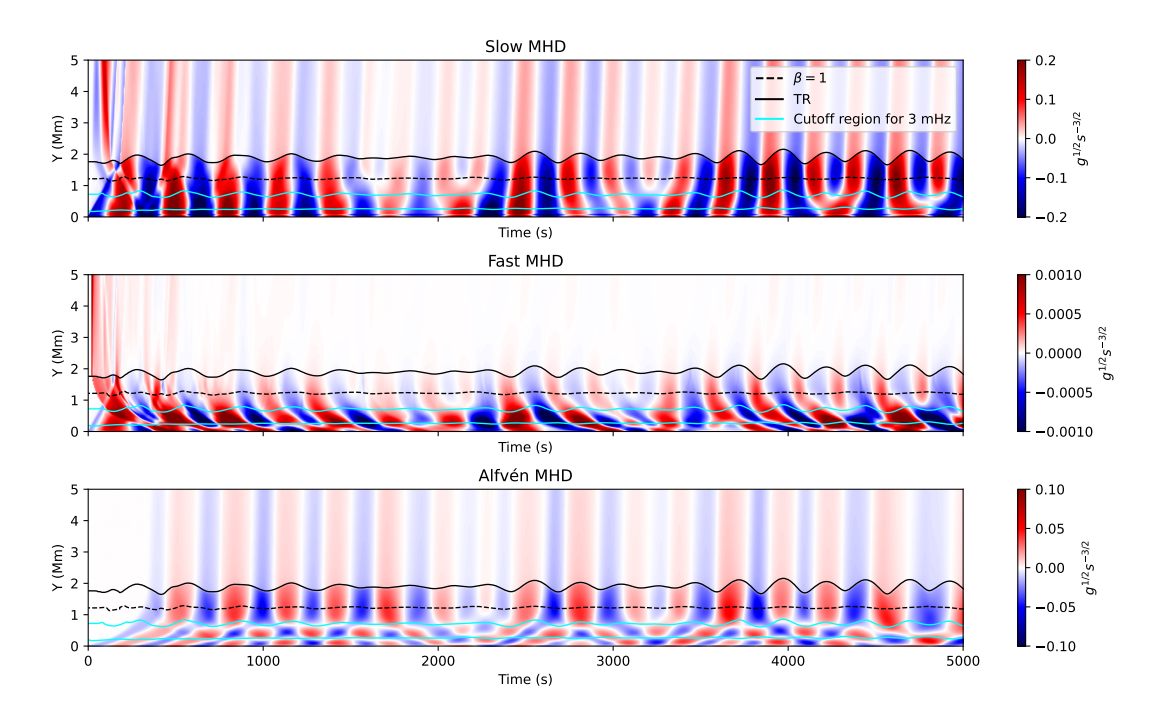


Figure 3.15: Temporal evolution of MHD wave variables at the center of the domain for an arcade magnetic field driven by a broadband source.

In the arcade magnetic field configuration, we observe a power spectrum qualitatively similar to the vertical magnetic field case, with a dominant peak at 3.2 mHz corresponding to the driver frequency. However, the Alfvén mode has a slightly more pronounced enhancement at the 4 mHz frequency compared to the vertical field case. This subtle difference can be attributed to the increased complexity and curvature of the magnetic field lines in the arcade configuration, which facilitates additional mode coupling and partial transmission of higher-frequency components.

Unlike the slow and fast modes, which exhibit more significant spectral changes due to reflections and mode conversion near the $\beta=1$ region and at the transition region, the Alfvén mode remains relatively unaffected. This is because our model is based on Cartesian coordinates and lacks transverse structuring along the z-axis (perpendicular to the 2D simulation plane), which limits the generation and interaction of torsional Alfvén waves, which require such structuring to develop fully. As a result, while we do detect a slight increase in Alfvénic power at 4 mHz, it is less dramatic compared to the modifications seen in the slow and fast mode spectra.

These results highlight the sensitivity of wave dynamics to the background magnetic geometry and dimensionality of the system. Incorporating transverse inhomogeneities or extending the model to 3D could potentially amplify Alfvén wave generation and mode conversion effects, as suggested by previous works (e.g., Cally and Thompson (2003), Doorsselaere et al. (2008)). The observed spectral behavior in both magnetic configurations reinforces the role of magnetic topology in governing wave propagation, energy transfer, and mode coupling in the structured solar atmosphere.

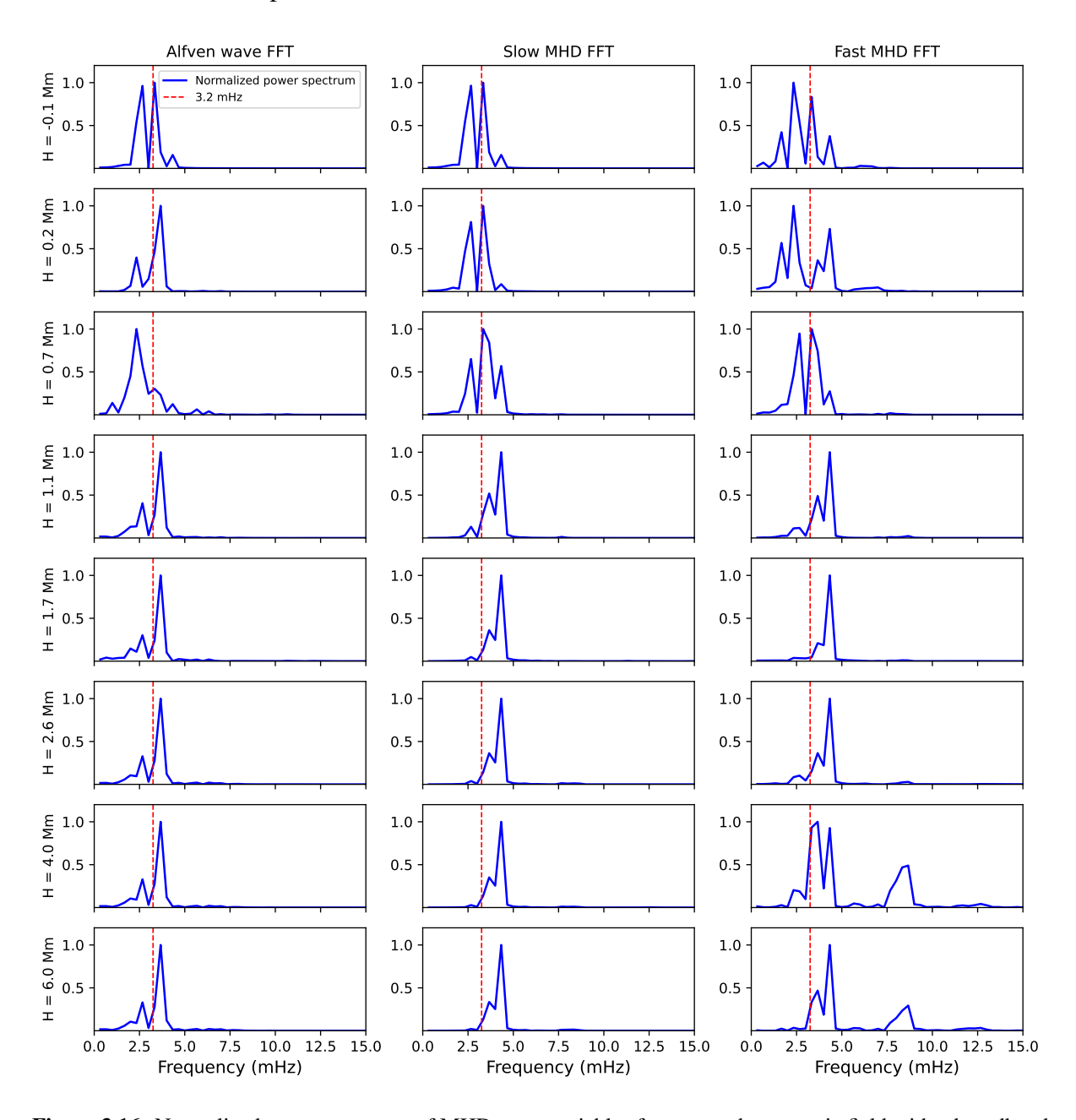


Figure 3.16: Normalized power spectrum of MHD wave variables for an arcade magnetic field with a broadband driver.

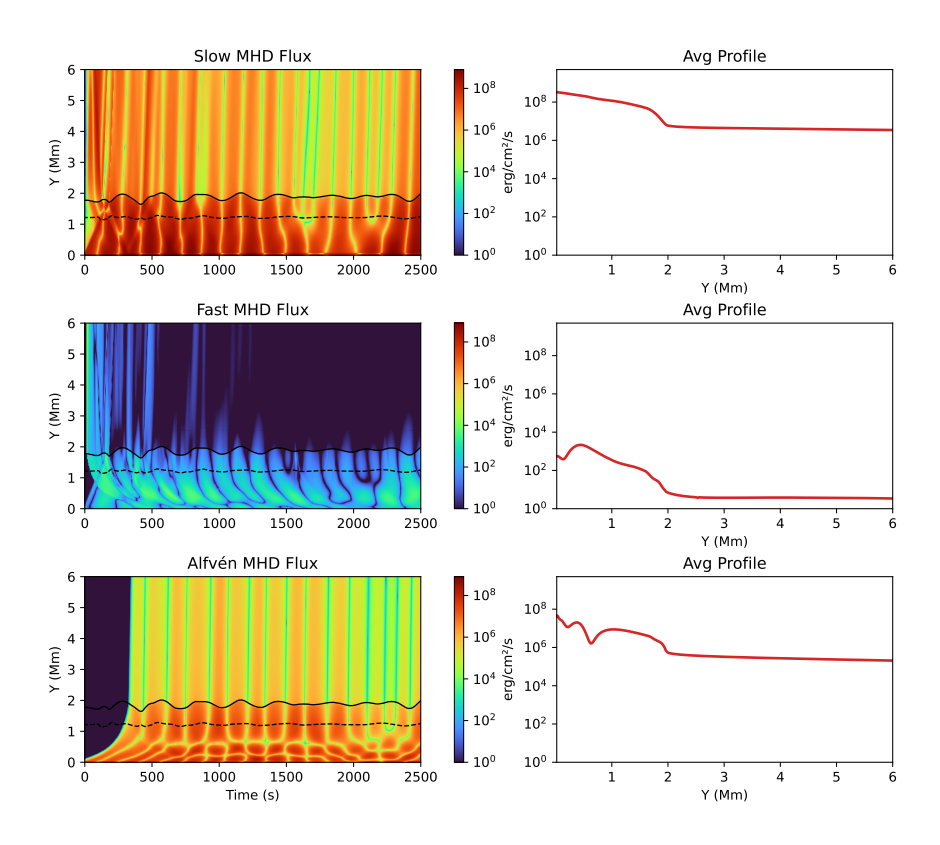


Figure 3.17: Energy flux components for slow, fast, and Alfvén modes in an arcade magnetic field driven by a broadband driver.

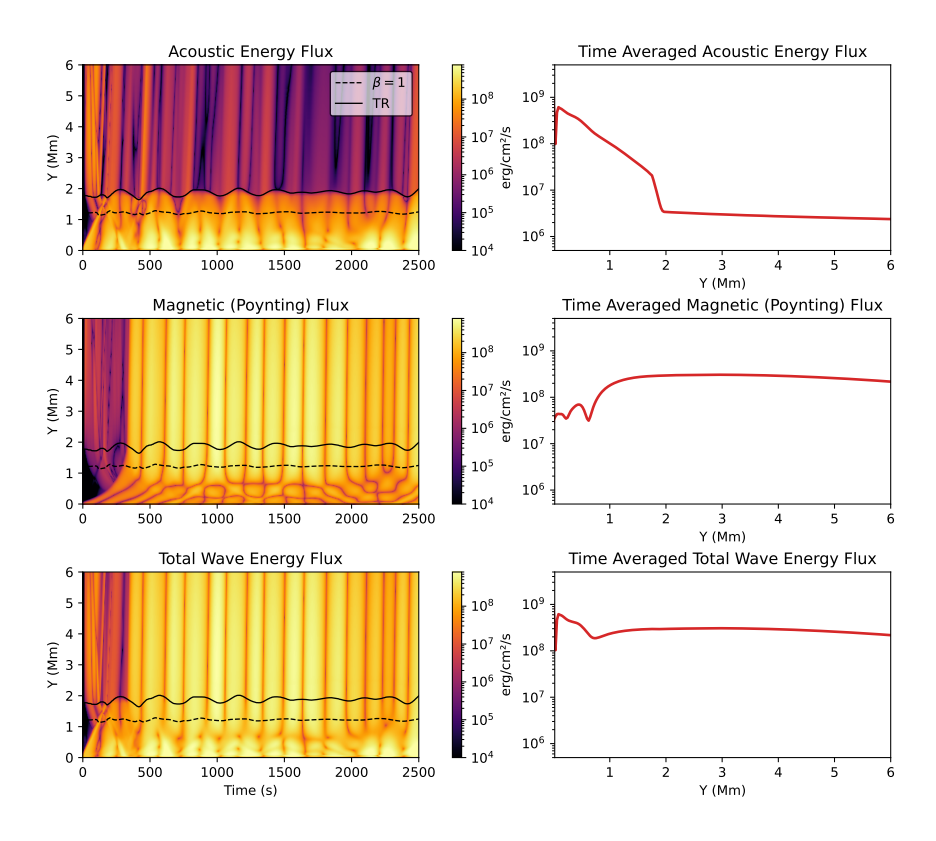


Figure 3.18: Acoustic, magnetic and total energy flux as a function of height for an arcade magnetic field with a broadband driver.

3.3 Transient events (Solar jets)

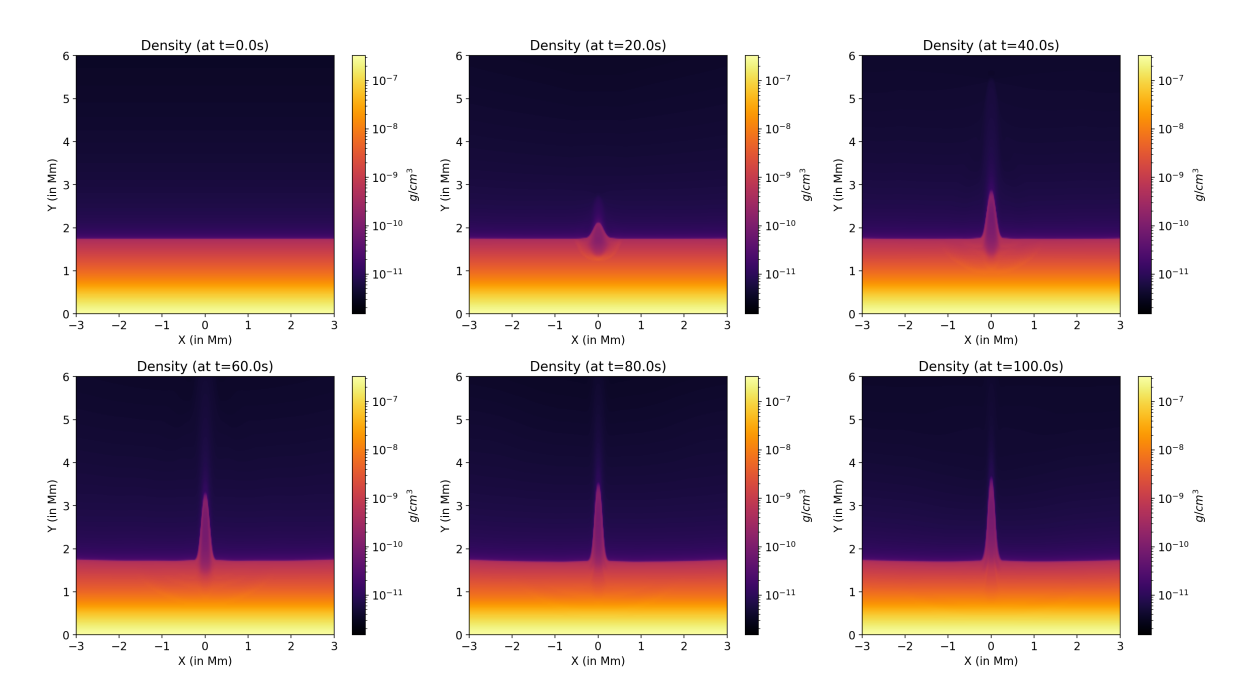


Figure 3.19: Time evolution of a solar jet driven by a pressure-pulse perturbation in an arcade magnetic field. The panels show the progression of the jet at successive time frames.

3.3.1 Solar Jet Launch and Wave Evolution

To investigate the plasma response to impulsive events in the solar atmosphere, a solar jet was initiated through a spontaneous pressure perturbation, as described in Section 2.3. The perturbation was applied with a spatial width of 100 km at a height of 1.6 Mm, locally elevating the plasma temperature from approximately 7,000 K to 60,000 K. This produced a jet attaining a peak upward velocity of 38 km s⁻¹. Owing to the isotropic nature of energy propagation in such transient events, waves were generated both upwards and downwards. The jet reached a maximum height of roughly 3.8 Mm. A relatively small-amplitude jet was deliberately chosen to minimize artificial reflections from the computational sponge layer.

As shown in Fig. 3.20, the jet launch excites both longitudinal and transverse MHD wave modes, with clear periodic signatures in their propagation. A particularly distinct feature appears near the $\beta=1$ layer, where a conversion of slow magnetoacoustic modes into fast modes is evident. The corresponding power spectrum reveals a dominant peak near 3.5 mHz, consistent with the typical lifetimes of solar jets, which generally span 3–5 minutes. Moreover, the transverse modes exhibit notable power at higher frequencies, indicative of multi-frequency wave activity generated during the jet's ascent.

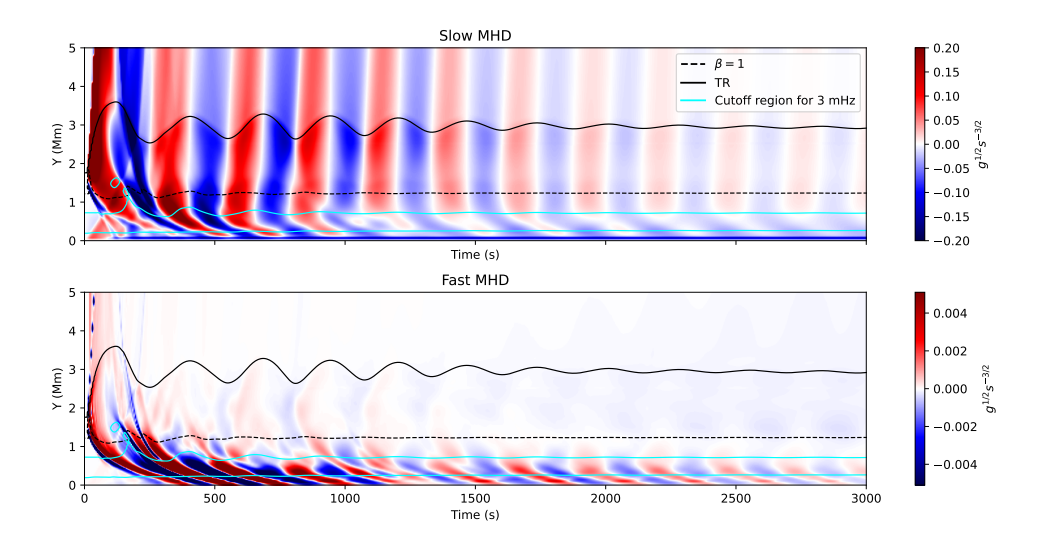


Figure 3.20: Temporal evolution of slow and fast MHD energy flux components following the launch of a jet in an arcade magnetic field without p-mode oscillations.

The power spectra of the fast magnetoacoustic modes, displayed in Fig. 3.23, further support these findings. Distinct peaks are evident, affirming the presence of wave reflections and frequency enhancement at characteristic atmospheric layers.

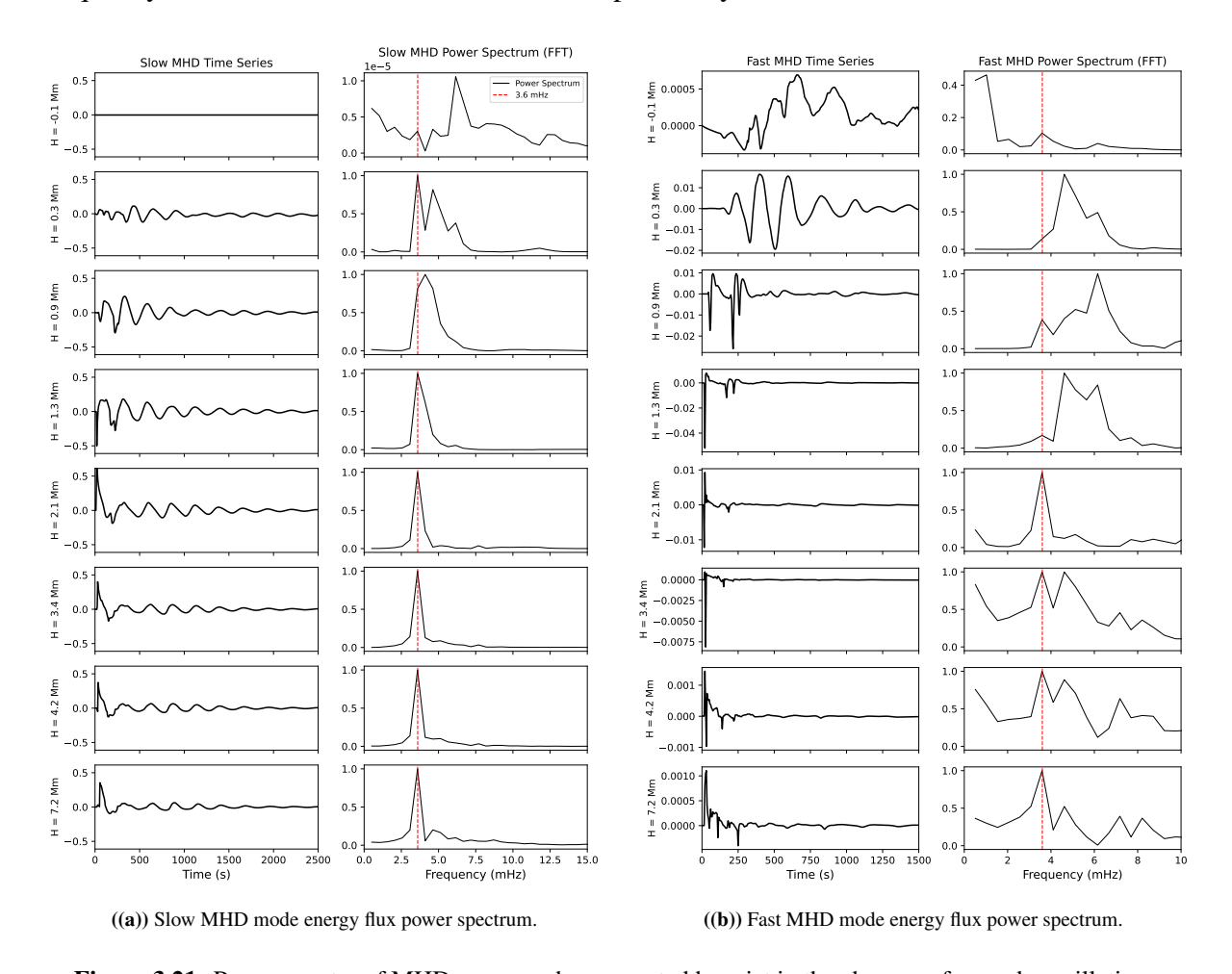


Figure 3.21: Power spectra of MHD wave modes generated by a jet in the absence of p-mode oscillations.

3.3.2 Solar Jets under the Influence of *p*-Mode Oscillations

In a complementary experiment, the effect of global p-mode oscillations on jet-driven wave activity was examined by introducing a monochromatic velocity driver at the lower boundary with a frequency of 3.2 mHz. The temporal evolution of the MHD wave fluxes is shown in Fig. 3.22. A clear modification in the behavior of the propagating waves is observed compared to the case without p-modes.

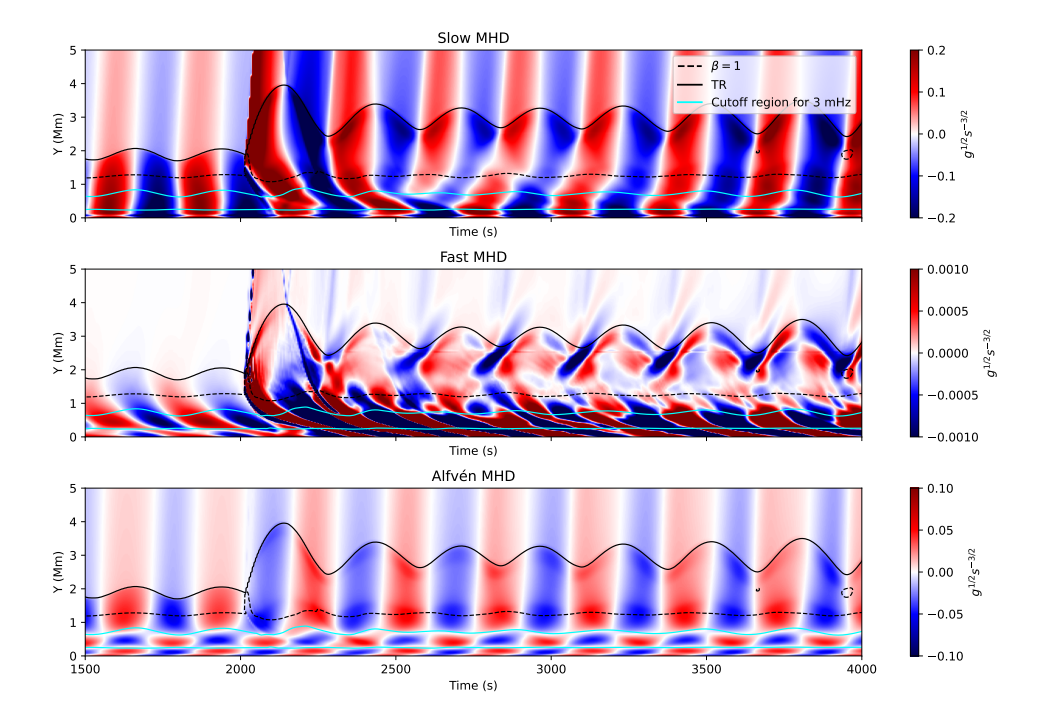


Figure 3.22: Temporal evolution of slow and fast MHD flux components for a jet launched in the presence of p-mode oscillations in an arcade magnetic field.

The imposed *p*-mode oscillations noticeably alter the power distribution within the system. The peak power shifts from 3.2 mHz (the driver frequency) to approximately 3.7 mHz, with an additional enhancement near 4 mHz. Furthermore, the jet apex exhibits a tendency to resonate with the imposed oscillations, modulating its trajectory over time.

A comparable trend is evident in the power spectra of the fast magnetoacoustic modes. At lower heights, particularly below the $\beta=1$ layer, the power spectra display additional high-frequency components. These can be attributed to wave trapping and partial reflections in the acoustic cutoff region, which enhance selected frequencies. At higher altitudes, distinct peaks around 7 mHz appear, likely resulting from partial reflections at the upper boundary despite the presence of sponge layers designed to suppress such effects.

These findings underscore the significant influence of global p-mode oscillations on jet dynamics and the resulting wave activity. The interplay between jet-driven perturbations and background oscillations not only modifies the dominant frequencies within the atmosphere but

also facilitates the generation of secondary high-frequency components through reflection and mode conversion processes at critical transition layers.

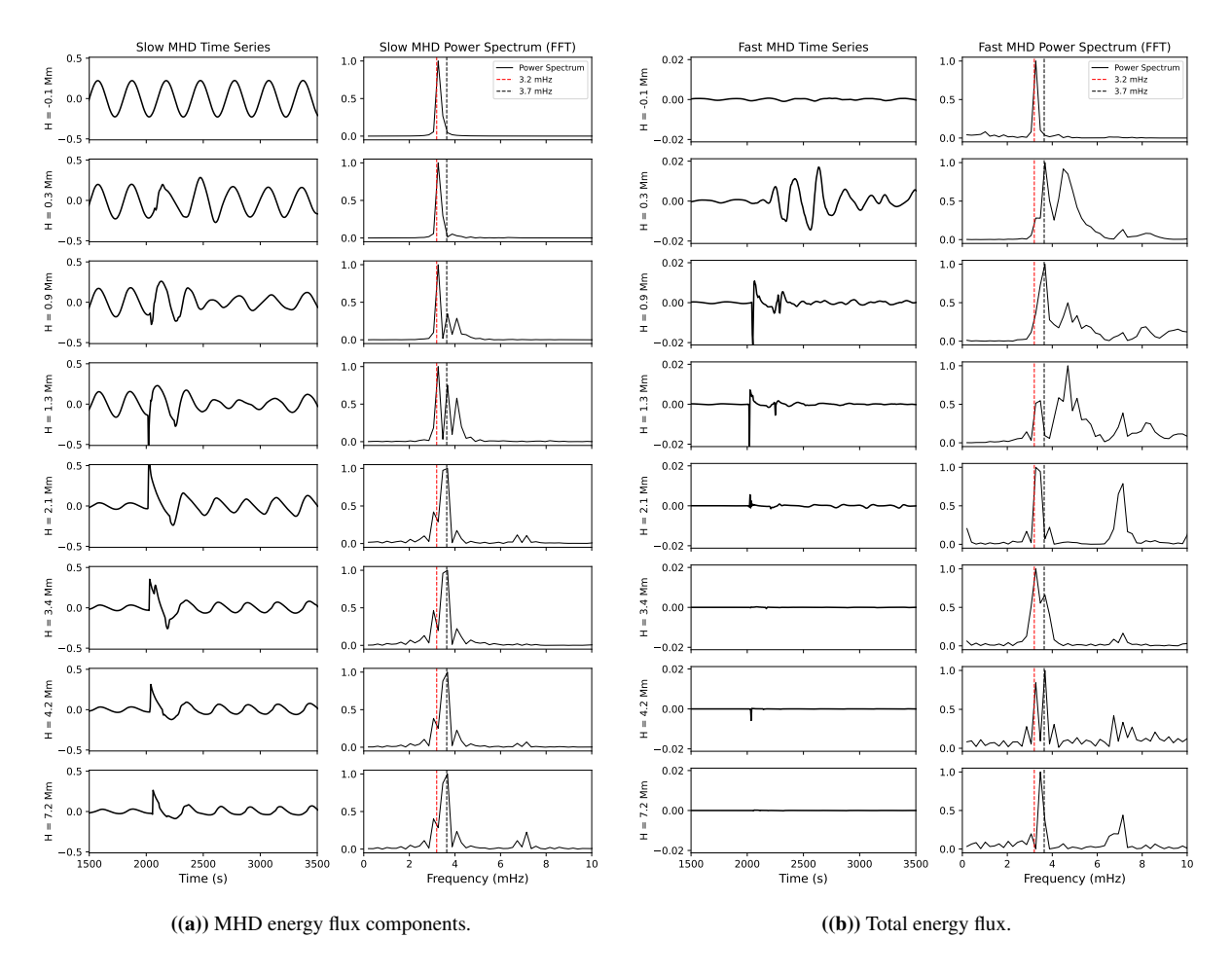


Figure 3.23: Power spectra for for slow and fast MHD components generated by jet launch along with p-mode oscillations.

Chapter 4

Summary & Outlook

4.1 Summary

We conducted a series of numerical experiments to investigate the propagation and evolution of MHD waves in different magnetic field configurations subjected to various photospheric drivers. We summarize our study as follows:

- We carried out numerical experiments by perturbing the velocity components v_y and v_z with both monochromatic and broadband drivers. The monochromatic driver had a frequency of 3.2 mHz, while the broadband driver was centered at 3.2 mHz and covered a range of frequencies (Fig.2.6).
- For the monochromatic driver, the power spectra of all three MHD wave modes exhibited a prominent peak at 3.2 mHz. Slow magnetoacoustic modes partially reflected at the transition region, fast modes were predominantly reflected below the corona, and Alfvén waves propagated upward with partial reflection and standing wave formation in the chromosphere. Acoustic energy remained confined to lower layers, while magnetic energy—primarily carried by Alfvén waves—was efficiently transmitted into the corona.
- The broadband driver introduced a redistribution of spectral power, causing a noticeable shift of the dominant power peak to around 4 mHz. This shift resulted from frequency-dependent reflection and cutoff processes. The arcade magnetic field configuration displayed qualitatively similar behavior to the vertical field but exhibited enhanced high-frequency power in the Alfvén mode.
- Simulations of pressure-driven solar jets without background p-mode oscillations produced both longitudinal and transverse waves with power peaking near 3.5 mHz, consistent with typical chromospheric jet lifetimes. The introduction of a monochromatic

p-mode driver shifted the spectral peak to approximately 3.7 mHz. The jet apex exhibited resonance with the imposed oscillations, while fast modes at lower heights displayed high-frequency enhancements likely associated with reflections within the acoustic cutoff region.

From these experiments, several key conclusions can be drawn:

- Both the nature of the photospheric driver and the background magnetic field configuration critically affect wave propagation, energy transport, and spectral behavior in the solar atmosphere.
- The addition of p-mode-like drivers enhances high-frequency transverse oscillations in the chromosphere, with implications for the dynamics of solar jets. This complements observational results by Morton et al. (2019); Tomczyk et al. (2007); Kuniyoshi et al. (2024a), who reported enhanced Alfvénic power in the 3–4 mHz range, hinting at a coupling between photospheric p-modes and coronal oscillations. This becomes extremely important as it is known that low frequency waves carry significant energy with them (Morton et al. (2025)).
- Our results echo those of Miriyala et al. (2025), who showed that dynamic driving plays a critical role in enhancing higher frequency oscillations at around 4 mHz. Their study demonstrated that the introduction of time-dependent, broadband driving profiles leads to increased power in the higher frequency range. Our findings reinforce this conclusion by revealing similar high-frequency amplification when introducing a broadband p-mode driver.
- There are certain limitations associated with the simulations that needs to be acknowledged. The two-dimensional geometry restricts the representation of fully three-dimensional wave mode coupling processes, particularly fast-to-Alfvén conversion, which depends on non-coplanar geometries. Furthermore, the idealized driving profiles, simplified boundary conditions, and absence of multi-fluid effects and comprehensive radiative transfer treatments constrain the physical realism of the modeled chromospheric dynamics.

4.2 Future Work

Current work can be expanded for future research by addressing several key areas:

• Three-Dimensional Simulations: Moving to 3D simulations will capture more complex wave propagation and mode conversion processes, particularly in low- β regions and the fast-to-Alfvén conversion in the upper atmosphere.

- Wave Decomposition: We have used a simplistic wave decomposition method for 2D simulation. However, in 3D, wave decomposition presents a greater challenge as we have infinite directions perpendicular to the magnetic field line. Notably, wave decomposition for flux tubes, which assumes an axisymmetrical configuration, has been employed and studied (Khomenko and Cally (2012); Skirvin and Van Doorsselaere (2024); Miriyala et al. (2025).)
- Energy Dissipation Models: Including advanced radiative transfer and wave heating mechanisms will improve our understanding of energy deposition in the corona and its role in coronal heating.
- Comparison with Observations: Direct comparison with observations from *SDO*, *Hinode*, and upcoming missions will help validate and refine the model, providing insights into wave-driven spicule oscillations and their contribution to solar atmospheric dynamics (Morton et al. (2019); Tomczyk et al. (2007)).
- Investigating energy flux in each frequency range: An important diagnosis we can do is to calculate the energy flux for different frequency range to understand the energy transport mechanism further as observations have shown that lower frequency shows predominant energy flux.

These directions will help refine our understanding of p-mode-driven waves and their impact on solar atmospheric processes, including coronal heating and spicule dynamics.

Bibliography

- Cally, P. S. (2006). Dispersion relations, rays and ray splitting in magnetohelioseismology. *Philosophical Transactions of the Royal Society A: Mathematical, Physical and Engineering Sciences*, 364(1839):333–349.
- Cally, P. S. and Goossens, M. (2008). Three-dimensional mhd wave propagation and conversion to alfvén waves near the solar surface. i. direct numerical solution. *Solar Physics*, 251:251–265.
- Cally, P. S. and Hansen, S. C. (2011a). Benchmarking fast-to-alfvén mode conversion in a cold magnetohydrodynamic plasma. *The Astrophysical Journal*, 738(2):119.
- Cally, P. S. and Hansen, S. C. (2011b). Benchmarking fast-to-alfvén mode conversion in a cold magnetohydrodynamic plasma. *The Astrophysical Journal*, 738(2):119.
- Cally, P. S. and Thompson, M. J. (2003). Mode conversion and reflection of alfvén waves in the solar atmosphere. *The Astrophysical Journal*, 586(1):553–565.
- Cranmer, S. R. and van Ballegooijen, A. A. (2005). On the generation, propagation, and reflection of alfvén waves from the solar photosphere to the distant heliosphere. *The Astrophysical Journal Supplement Series*, 156(2):265–293.
- De Moortel, I., Falconer, I., and Stack, R. (2020). Alfvén on heating by waves. *Astronomy Geophysics*, 61(2):2.34–2.39.
- De Pontieu, B., Erdélyi, R., and James, S. P. (2004). Solar chromospheric spicules from the leakage of photospheric oscillations and flows. *Nature*, 430:536–539.
- de Pontieu, B., McIntosh, S., Hansteen, V. H., Carlsson, M., Schrijver, C. J., Tarbell, T. D., Title, A. M., Shine, R. A., Suematsu, Y., Tsuneta, S., Katsukawa, Y., Ichimoto, K., Shimizu, T., and Nagata, S. (2007). A Tale of Two Spicules: The Impact of Spicules on the Magnetic Chromosphere. , 59:S655.
- De Pontieu, B., McIntosh, S. W., Carlsson, M., Hansteen, V. H., Tarbell, T. D., Schrijver, C. J., Title, A. M., Shine, R. A., Tsuneta, S., Matsuzaki, K., Nagata, S., Shimizu, T., Suematsu,

- Y., Ichimoto, K., Katsukawa, Y., Tarbell, T. D., and Shine, R. A. (2007). Chromospheric alfvénic waves strong enough to power the solar wind. *Science*, 318(5856):1574–1577.
- Dedner, A., Kemm, F., Kröner, D., Munz, C.-D., Schnitzer, T., and Wesenberg, M. (2002). Hyperbolic divergence cleaning for the mhd equations. *Journal of Computational Physics*, 175:645–673.
- Dey, S., Chatterjee, P., O. V. S. N., M., Korsós, M. B., Liu, J., Nelson, C. J., and Erdélyi, R. (2022). Polymeric jets throw light on the origin and nature of the forest of solar spicules. *Nature Physics*, 18(5):595–600.
- Doorsselaere, T. V., Goossens, M., and Moortel, I. D. (2008). Detection of waves in the solar corona: Kink or alfvén? *The Astrophysical Journal Letters*, 676(1):L73–L75.
- Eddy, J. A. and Ise, R. (1979). *New Sun: The Solar Results From Skylab. NASA SP-402*, volume 402.
- Edlén, B. (1942). Identification of fe xiv in the solar corona. *Astrophysical Journal*, 95:356–358. Edlén's work marked a breakthrough in understanding coronal temperatures by identifying ionized iron in the corona.
- Elsworth, Y., Broomhall, A.-M., Gosain, S., Roth, M., Jefferies, S., and Hill, F. (2015). The importance of long-term synoptic observations and data sets for solar physics and helioseismology. *Space Science Reviews*, 196.
- Felipe, T., Khomenko, E., and Collados, M. (2010). Magneto-acoustic Waves in Sunspots: First Results From a New Three-dimensional Nonlinear Magnetohydrodynamic Code., 719(1):357–377.
- Gao, Y., Guo, M., Van Doorsselaere, T., Tian, H., and Skirvin, S. J. (2023). Modeling of Transverse Oscillations Driven by p-modes in Short Coronal Loops., 955(1):73.
- Gary, G. A. (2001). Plasma Beta above a Solar Active Region: Rethinking the Paradigm., 203(1):71–86.
- Gibson, S. E. and Fan, Y. (2006). Coronal prominence structure and dynamics: A magnetic flux rope interpretation. *Journal of Geophysical Research: Space Physics*, 111(A12).
- Gomez, D. O., Dmitruk, P. A., and Milano, L. J. (2000). Recent theoretical results on coronal heating. *Solar Physics*, 195:299–318. Received 20 September 1999; accepted 1 March 2000.
- Hansen, S. C. and Cally, P. S. (2012). Benchmarking fast-to-alfvén mode conversion in a cold mhd plasma. ii. how to get alfvén waves through the solar transition region. *The Astrophysical Journal*, 751(1):31.

- Heggland, L., De Pontieu, B., and Hansteen, V. H. (2007). Numerical Simulations of Shock Wave-driven Chromospheric Jets., 666(2):1277–1283.
- Jefferies, S. M., McIntosh, S. W., Armstrong, J. D., Bogdan, T. J., Cacciani, A., and Fleck, B. (2006). Magnetoacoustic portals and the basal heating of the solar chromosphere. *The Astrophysical Journal*, 648(2):L151–L154.
- Jess, D. B., Reznikova, V. E., Van Doorsselaere, T., Keys, P. H., and Mackay, D. H. (2013). The Influence of the Magnetic Field on Running Penumbral Waves in the Solar Chromosphere. , 779(2):168.
- Khomenko, E. and Cally, P. S. (2012). Numerical simulations of conversion to alfvén waves in sunspots. *The Astrophysical Journal*, 746(1):68.
- Khomenko, E., Collados, M., and Felipe, T. (2008). Nonlinear numerical simulations of magneto-acoustic wave propagation in small-scale flux tubes. *Solar Physics*, 251(1):589–611.
- Kuniyoshi, H., Shoda, M., Morton, R. J., and Yokoyama, T. (2024a). Can the Solar p-modes Contribute to the High-frequency Transverse Oscillations of Spicules?, 960(2):118.
- Kuniyoshi, H., Shoda, M., Morton, R. J., and Yokoyama, T. (2024b). Can the Solar p-modes Contribute to the High-frequency Transverse Oscillations of Spicules?, 960(2):118.
- Lamb, H. (1909). On the theory of waves propagated vertically in the atmosphere. *Proceedings* of the London Mathematical Society, s2-7(1):122–141.
- Leibacher, J. W. and Stein, R. F. (1981). Oscillations and pulsations. 450:263–287.
- Leighton, R. B., Noyes, R. W., and Simon, G. W. (1962). Velocity Fields in the Solar Atmosphere. I. Preliminary Report., 135:474.
- Liu, W. and Ofman, L. (2014). Advances in observing various coronal euv waves in the sdo era and their seismological applications (invited review). *Solar Physics*, 289:3233–3277.
- Low, B. C. (1985). Three-dimensional structures of magnetostatic atmospheres. I Theory. , 293:31–43.
- Mignone, A., Bodo, G., Massaglia, S., Matsakos, T., Tesileanu, O., Zanni, C., and Ferrari, A. (2007). PLUTO: A Numerical Code for Computational Astrophysics. *The Astrophysical Journal Supplement Series*, 170(1):228–242.

- Miriyala, H., Morton, R. J., Khomenko, E., Antolin, P., and Botha, G. J. (2025). The coronal power spectrum from mhd mode conversion above sunspots. *The Astrophysical Journal*, 979(2):236.
- Morton, R. J., Molnar, M., Cranmer, S. R., and Schad, T. A. (2025). High-frequency Coronal Alfvénic Waves Observed with DKIST/Cryo-NIRSP., 982(2):104.
- Morton, R. J., Tomczyk, S., and Pinto, R. (2015). Investigating alfvénic wave propagation in coronal open-field regions. *Nature Communications*, 6(7813). Open access.
- Morton, R. J., Weberg, M. J., and McLaughlin, J. A. (2019). A basal contribution from p-modes to the alfvénic wave flux in the sun's corona. *Nature Astronomy*, 3:223–229.
- Newington, M. E. and Cally, P. S. (2010). Reflection and conversion of magnetogravity waves in the solar chromosphere: windows to the upper atmosphere. *Monthly Notices of the Royal Astronomical Society*, 402(1):386–394.
- Okamoto, T. J. and De Pontieu, B. (2011). Propagating waves along spicules. *The Astrophysical Journal Letters*, 736(2):L24. Published 2011 July 5.
- Popescu Braileanu, B. and Keppens, R. (2021). Effects of ambipolar diffusion on waves in the solar chromosphere. , 653:A131.
- Powell, K. G. (1994). Approximate riemann solver for magnetohydrodynamics (that works in more than one dimension). Technical report, University of Michigan.
- Priest, E. (2014). Magnetohydrodynamics of the Sun.
- Priest, E. (2019). Chapter 7 magnetohydrodynamics and solar dynamo action. In Engvold, O., Vial, J.-C., and Skumanich, A., editors, *The Sun as a Guide to Stellar Physics*, pages 239–266. Elsevier.
- Priest, E. R. (1982). Solar Magnetohydrodynamics. Reidel Publishing Company, Dordrecht.
- Rajaguru, S. P., Sangeetha, C. R., and Tripathi, D. (2019). Magnetic fields and the supply of low-frequency acoustic wave energy to the solar chromosphere. *The Astrophysical Journal*, 871(2):155.
- Roberts, B. (2006). Slow magnetohydrodynamic waves in the solar atmosphere. *Philosophical Transactions of the Royal Society A: Mathematical, Physical and Engineering Sciences*, 364(1839):447–460.

- Samanta, T., Tian, H., Yurchyshyn, V., Peter, H., Cao, W., Sterling, A. C., Erdélyi, R., Ahn, K., Feng, S., Utz, D., and Banerjee, D. (2019). Generation of solar spicules and subsequent atmospheric heating. *Science*, 366(6467):890–894.
- Santamaria, I. C., Khomenko, E., and Collados, M. (2015). Magnetohydrodynamic wave propagation from the subphotosphere to the corona in an arcade-shaped magnetic field with a null point. *Astronomy & Astrophysics*, 577:A70.
- Schrijver, C. J., Hagenaar, H. J., and Title, A. M. (1997). On the patterns of the solar granulation and supergranulation. *The Astrophysical Journal*, 475(1):328–337.
- Singh, B., Sharma, K., and Srivastava, A. K. (2019). On modelling the kinematics and evolutionary properties of pressure-pulse-driven impulsive solar jets. *Annales Geophysicae*, 37:891–902.
- Siu-Tapia, A., Lagg, A., Solanki, S. K., and van Noort, M. (2019). Superstrong photospheric magnetic fields in sunspot penumbrae. *Astronomy and Astrophysics*, 631:A99.
- Skirvin, S., Verth, G., González-Avilés, J. J., Shelyag, S., Sharma, R., Guzmán, F. S., Ballai, I., Scullion, E., Silva, S. S., and Fedun, V. (2023). Small-scale solar jet formation and their associated waves and instabilities. *Advances in Space Research*, 71(4):1866–1892. Recent progress in the physics of the Sun and heliosphere.
- Skirvin, S. J. and Van Doorsselaere, T. (2024). Mode conversion and energy flux absorption in the structured solar atmosphere. , 683:A61.
- Srivastava, A. K., Shetye, J., Murawski, K., Doyle, J. G., Stangalini, M., Scullion, E., Ray, T., Wójcik, D. P., and Dwivedi, B. N. (2017). High-frequency torsional alfvén waves as an energy source for coronal heating. *Scientific Reports*, 7(1):43147.
- Tomczyk, S., Card, G. L., Darnell, T., Elmore, D. F., Lull, R., Nelson, P. G., Streander, K. V., Burkepile, J., Casini, R., and Judge, P. G. (2008). An instrument to measure coronal emission line polarization. *Solar Physics*, 247(2):411–428.
- Tomczyk, S., McIntosh, S. W., Keil, S. L., Judge, P. G., Schad, T., Seeley, D. H., and Edmondson, J. (2007). Alfven Waves in the Solar Corona. 2007:SH21A–0289.
- Tomczyk, S., McIntosh, S. W., Keil, S. L., Judge, P. G., Schad, T., Seeley, D. H., and Edmondson, J. (2007). Alfvén waves in the solar corona. *Science*, 317(5842):1192–1196.
- Ulmschneider, P. (1998). Heating of Chromospheres and Coronae. *Highlights of Astronomy*, 11A:831.

- Ulrich, R. K. (1970). The Five-Minute Oscillations on the Solar Surface., 162:993.
- Van Doorsselaere, T., Nakariakov, V. M., and Verwichte, E. (2008). Detection of waves in the solar corona: Kink or alfvén? *The Astrophysical Journal*, 676(1):L73–L76.
- Vernazza, J. E., Avrett, E. H., and Loeser, R. (1981). Structure of the solar chromosphere iii. models of the euv brightness components of the quiet sun. *The Astrophysical Journal Supplement Series*, 45:635–725. Copyright is not claimed for this article.
- Yadav, N., Keppens, R., and Popescu Braileanu, B. (2022). 3d mhd wave propagation near a coronal null point: New wave mode decomposition approach. *Astronomy & Astrophysics*, 660:A21.